PRELIMINARY DRAFT

COO - 818 - 87

H.C. $3.00; MN .75

AN EXPERIMENTAL TEST OF THE LAW OF BARYON CONSERVATION.

A Thesis Submitted to
Case Institute of Technology
In Partial Fulfillment of the Requirements
for the Degree of
Doctor of Philosophy

by
Henry S. Gurr

November 1966

Thesis Advisor:
Professor F. Reines.

DISCLAIMER

ABSTRACT

A 162 m^2 steradian scintillation detector located 3200 m below surface was used to look for high energy fragments from baryon non-conserving nucleon decay. A lower limit on the lifetime of the nucleon from 2 x 10^{28} to 8 x 10^{29} years, depending on the assumed decay mode, is established.

ACKNOWLEDGEMENTS

The author wishes to thank his thesis advisor, Professor F. Reines, for suggesting this problem and making possible its solution.

Thanks go to the members of the Case-Wits Neutrino Group, especially Drs. M. Crouch, T. Jenkins, J. Sellschop, W. Kropp, and Messrs. B. Meyer, H. Sobel, A. Hruschka, and B. Shoffner, for their vital contributions to the experiment.

The financial support of the U.S. Atomic Energy Commission, the hospitality of the Directors of the East Rand Proprietory Mine, and the willing assistance of the E.R.P.M. staff is gratefully acknowledged.

Finally the author wishes to thank his wife, Suzanne, for her continued help and encouragement.

TABLE OF CONTENTS

INTRODUCTION.

The law or principle of baryon* conservation, which asserts that in any transformation the number of baryons minus the number of antibaryons remains a constant, was first formulated as the law of conservation of nucleons by Stückelberg[1] and Wigner[2] and later evolved into its present form as the hyperons or "heavy baryons" were discovered. As is true with all physical laws, there is continued interest in testing the range of validity of the baryon conservation law, hence the present investigation.

The law has been found valid in innumerable direct observations of reactions between particles and no violations have been reported. Experiments which demonstrate the absence of nucleon decay** provide a more stringent test of the law. The stability of the nucleon and therefore our very existence*** is a

---

* Baryons are strongly interacting fermions with mass equal to or greater than that of the proton.

** In these discussions the term nucleon decay excludes ordinary beta decay since this process conserves baryons.

*** From this one may immediately deduce that the nucleon lifetime is greater than the age of the universe which is estimated to be $\sim 10^{10}$ years. From very simple measurements of the ambient level of radioactivity one can deduce that the nucleon lifetime is greater than 10^{17} years.

non-trivial fact, implying the existence of a fundamental principle, since there is apparently no other reason why the nucleon does not decay. The law of baryon conservation is thus thought to be directly responsible for the stability of nucleons, since it follows as a consequence that the decay of a nucleon into lighter and therefore non-baryonic particles may not occur.

Table I summarizes the results of previous experiments which have sought to detect nucleon decay. These experiments have been able to specify only a lower nucleon lifetime limit* for specific modes of nucleon decay. The effect of the nuclear binding on the lifetime is assumed to be unimportant in view of the relatively small binding energy as compared with the nucleon rest mass.

This thesis sets new and more stringent nucleon lifetime limits for modes of decay which produce high energy ionizing particles, and follows the techniques and spirit of those who previously[3-8] used the method.

---

* Lifetimes are here used as a convenient expression to relate the observed rate of events to the nucleon decay sensitivity of the detector. There is no implication that the concept of time, as we know it, is valid on the scale of 10^{20} years.

The results are based on measurements made in conjunction with the Case-Wits* Neutrino Experiment. The apparatus was a $162m^2$ steradian scintillation detector located 3200 meters below the surface in a gold mine near Johannesburg, South Africa. The experiment differs from those which precede it primarily in the large size of the detector and the greatly reduced cosmic ray background associated with the extreme depth of the apparatus.

HIGH ENERGY DECAY FRAGMENT METHOD.

Nucleons in a given sample of material are presumed to decay into high energy ionizing particles in a manner which obeys all conservation laws except baryon and lepton conservation.** The experimenter sets out to detect these particles, and from the rate of observed events and the detector configuration he deduces the nucleon lifetime or, if the events cannot

---

* Case Institute of Technology, Cleveland Ohio, U.S.A.
University of the Witwatersrand, Johannesburg, South Africa.

** It is seen that the decay of the nucleon to known particles is not possible if only the baryon conservation constraint is relaxed.

be clearly ascribed to nucleon decay, a lower nucleon lifetime limit.

In this thesis several plausible nucleon decay modes, (See Table II) consistant with the conservation of energy, momentum, spin, and charge, are chosen as examples upon which to base quantitative results. The lifetime limits based on these modes are representative of the limits which would be true for any decay mode involving ionizing decay particles. It is recognised, however, that the charged particle or particles from events of very high particle multiplicity might not have sufficient energy to be detected. The particle energies listed in Table II follow from the application of energy and momentum conservation to the decay of a free nucleon.

In the case of an initially bound nucleon, the residual nucleus can carry off ~10-20 MeV in its recoil and hence a bound nucleon decay particle can have an energy less than that from a free nucleon. Since such accuracy is not warranted here, the difference is ignored and the energies listed in Table II are assumed to apply to all nucleons.

EXPERIMENTAL REQUIREMENTS.

The experimental arrangement is that of a detector in an underground cavity, shown schematically in Fig. 1. The nucleons whose decay is sought are in the detector itself and within the walls of the cavity. The nucleons in the walls which might contribute events in the detector are within a shell having a thickness equal to the range of the decay particles.

Equation I* relates the nucleon lifetime to experimental quantities. It is seen that the nucleon decay counting rate from nucleons of lifetime greater than 10^{28} years will be very low even with a large detector.

$$\tau = \frac{N_{eff}}{\frac{(\Delta N)}{(\Delta t)}} \qquad (1)$$

τ = nucleon mean lifetime.**

$N_{eff} = n_d V_{eff} + n_w R_w A_{eff}$ = Effective Number of Nucleons.

---

* Equation I is valid for one ionizing decay particle. This and other more complicated cases are considered in Appendix I, II and III.

** All numerical results are expressed in lifetime $T_{\frac{1}{2}}$ units where $T_{\frac{1}{2}} = \ln 2\, \tau$.

$\left(\frac{\Delta N}{\Delta t}\right)$ = nucleon decay event rate due to one ionizing fragment.

R_w = range of decay fragment.

n_d = number of nucleons per unit volume in detector.

n_w = number of nucleons per unit volume in walls of cavity.

A_{eff} = effective area of detector = shadow area of detector averaged over all angles.

V_{eff} = effective volume of detector = detector volume within which decay is detected with 100% efficiency.

This equation embodies the general and rigorous result that the response of a detector in a cavity with thick homogenious walls is independent of the shape or size of the cavity. It is interesting to note that for a given detector the maximum effective number of nucleons is achieved with the detector-cavity arrangement.

DESCRIPTION AND OPERATION OF THE DETECTOR.

The detector has been described elsewhere,[10, 11] and only a brief description will be given here.* It

* The 6 detector elements comprising Bay 1 were set into operation on 27 October, 1964. The area of the system was increased one bay at a time until all nine bays were operating on 26 November, 1965.

consisted of 54 scintillation detector elements, each (Fig. 2) consisting of a long clear lucite plastic box filled with a mineral oil based scintillator and viewed by two photomultiplier tubes on each end. The detector elements (Fig. 3) were arranged end to end in six discontinuous rails, three rails on each side of a long horizontal tunnel.* The geometry of the array was chosen to provide the largest possible area and a crude angular resolution for the detection of particles penetrating at zenith angles greater than 45 degrees. The thickness of the detector elements was chosen so that a penetrating charged particle would deposit at least 20 MeV. Separate and identical electronic recording systems were provided for the East and West sides of the detector array.

The electronic recording systems operated in the following manner. A particle depositing energy in a single detector element would cause an output pulse from each of the four photomultiplier tubes (P.M.) on that detector. These pulses were passed through a

* Access to one end of the tunnel was by a 60 degrees (to zenith) inclined main haulage shaft, which communicated with other parts of the mine.

coding system (Fig. 4) to a four-fold coincidence circuit and to an oscilloscope recording camera (Fig. 5). The four-fold coincidence triggering threshold was set so that any ionizing particle depositing $\gtrsim$ 10 MeV in any element would trigger both East and West recording systems. The photographic record included the following data: the designation of the element or elements in which sufficient energy had been deposited, the pulse height and pulse shape produced by each P.M. tube, and the relative timing of each pulse (to within $\pm$ 0.2 microseconds). Pulses from the simultaneous penetration of more than one element on the same side were combined into one record* but pulses from each side of the detector East and West were recorded separately. The pulses from the detector were analysed to determine the position of the event along the length of the detector and the amount of energy deposited. Energy resolution was estimated to be $\sim \pm$ 20 percent. The desire to obtain the largest area for the available resources precluded measures to

---

* In a few cases, where on one side of the array elements in more than one bay were penetrated, the coding system did not permit all pulse heights to be determined unambiguously.

improve energy resolution.

An individual scintillation detector, identical to those below ground, was located on the surface. In this detector pulses from a radioactive source were compared with those from penetrating cosmic ray muons. The source was in turn used to calibrate each of the detectors below ground. The energies assigned to observed events by this calibration scheme are consistent with the energies expected from minimum ionizing particles.

To insure continuous sensitivity, the system was regularly tested with an automatic sequencing light pulser. (See Appendix V). A light pulse, very similar to that from an actual scintillation pulse, was directed into each detector element, and the resulting pulses were recorded by the cameras in exactly the same manner as an event. The energy threshold of the system was so set that background pulses from natural radioactivity which deposited energy immediately in front of the phototubes could accidently meet the four-fold coincidence requirement and regularly trigger the recording system. These pulses provided an additional check on the sensitivity of the system

but were readily distinguished from penetrating particles either because the four pulses did not originate in the same tank or because the energy deposited was too small.

OBSERVED EVENTS.

The features of the observed events are here compared with those expected from the modes of nucleon decay listed in Table II. Table III lists the deposited energy, time, position, and angle of penetration of the observed events which involve only one detector element on each side of the detector array. Table IV lists the number of events which involve one, two, and three detector elements on one side of the detector array. In addition ten events were observed which involved more than one detector element on each side of the detector array. These events were rejected as not being consistent with nucleon decay.

A) Time and Position.

Nucleon decay events should occur at random times and be distributed uniformly throughout the various regions of the detector. The observed

events are consistent with these two criteria.

B) Deposited Energy (Particle Penetrating One Tank on Each Side of Detector Array).

Since the detectors are thin compared to the range of the postulated nucleon decay fragments,* they are in most cases able to measure only the ionization of the decay fragment somewhere along its range and not the total energy of the fragment. Thus the observed particles may have an energy greater than the observed deposited energy, which on the average, totals about 50 MeV. The predominance of events with energy deposited in each detector near that expected from the penetration of a minimum ionizing particle (approximately 25 MeV), suggests that the observed particles have an energy greater than 150 MeV. The observed deposited energies are consistent with nucleon decay, but it is not possible to distinguish nucleon decay events from those in which other higher energy ionizing particles may also be present (e.g. neutrino induced muons).

C) Deposited Energy (Near Vertical Events).

A vertically travelling ionizing particle deposits

* An exception being the kaon.

maximum energy in a single detector if it is stopped within that detector. For a muon, pion, and kaon, this energy is respectively 140, 150 and 240 MeV. For an electron decay fragment the vertical depth of the detector element is slightly less than the electron shower range. Thus the detectors do not have sufficient thickness in the vertical direction to measure the energy of the muon, pion or electron nucleon decay fragments and distinguish them from other ionizing particles which may also be present (e.g. cosmic ray muons). Higher energies could be measured for particles passing through 2 or 3 detectors in a near vertical direction or passing along the length of the detector, but the aperture for such events is small. Since the deposited energies for 1, 2 and 3 detector near vertical events are highly dependent on the angle and position of penetration, (making it difficult to predict what energy distribution to expect), no detailed discussion will be attempted. The events, with deposited energy greater than 110 MeV total are not consistent with proton to kaon decay. All other events are taken to be consistent with nucleon decay.

D) Angle of Penetration.

It is reasonable to assume that if nucleon decay occurs it will give rise to products which have no preferred axis and hence on the average will be isotropically distributed at the point of decay.* As is shown in Appendix II it follows from this assumption that the rate of nucleon decay coincidence events in a pair of detectors is proportioned to the aperture** of the pair.*** Therefore if the observed events arise entirely from nucleon decay the intensity, which is the ratio of the rate of observed events to the aperture, should be nearly the same for all pairs of detectors.

To facilitate a test of this criterion, the

---

* The existence of an angular correlation of the decay products with each other would not invalidate this assumption.

** The aperture for a pair of detectors is the solid angle subtended by one detector at an element of area of the other detector integrated over all the elements of area. See Appendix III for an exact formulation and solution of the integral.

*** From which it follows that the flux of nucleon decay fragments within the cavity is homogeneous and isotropic.

detector elements are grouped into the pairs of discontinuous rails shown in Fig. 6 through 11. Identical pairs which define the same angular range are grouped into the Classes shown in this figure. In Table V the rate of observed events, aperture, and intensity for each class is given. It is seen that the intensity of events is not the same, showing a departure from isotropy and hence the presence of <u>non nucleon</u> decay particles. The significantly greater intensity in the vertical direction is due to the presence of cosmic ray muons from the atmosphere. Indeed it is reasonable to conclude that almost all of the events in classes IV, V and VI are due to cosmic rays, but the argument can not be made quantative from these data alone. As is discussed below, a large fraction of the events in Classes I, II, and III are from neutrino interactions. The intensity for Class I is slightly greater than that for Class II and III, as expected from neutrinos, but the data to date are statistically uncertain and the distribution within Classes I, II and III is consistent with isotropy. The cosmic ray and neutrino events serve as a background in the present experiment.

CALCULATION OF NUCLEON LIFETIME LIMITS.

Since no feature of the observed events clearly indicates the presence of nucleon decay, only a lower limit on the nucleon lifetime can be obtained from the present experiment. It was decided to base the results on the event rate in Classes I, II and III since this avoids the considerable uncertainties in estimating the contribution due to the cosmic ray background and also gives the highest lower limit. The lower lifetime limit for each decay mode listed in Table II is calculated in two different ways and the results are given in Table VI. The lifetime for each mode is calculated on the assumption that all of the events, not attributable to other causes and consistent with the mode, are due to nucleon decay in that mode alone. All calculations were based on Equations 11 and 17.

A) Nucleon Lifetime Consistent with Events in Class III (Background not Subtracted).

It is seen from Table V that the number of events per unit aperture is lowest in Class III. Since no events occurred in this Class, the rate was arbitrarily taken to be one event in the period of observation. If all of the events in Table II are assumed to be from nucleon decay, then the most favorable lifetime limits are obtained from Class III yielding the (background not subtracted) results in Table VI.

B) Nucleon Lifetime Consistent with Events in Class I, II and III (Neutrino Induced Muons Subtracted).

Almost all of the events in Classes I, II and III are due to muon neutrino interactions in the rock surrounding the detector and are, of course, the events for the detection of which the apparatus was designed. Using the muon neutrino rates predicted for this detector,[11] no fewer than eight of the events in Table III are due to neutrinos. It would thus seem reasonable that no more than four of the events in Table III are due to nucleon decay thus yielding the results in Table VI.

CONCLUSIONS.

The data give no evidence for the existence of high energy fragments from nucleon decay. Lower limits on the lifetime of the nucleon from 2×10^{28} to 8×10^{29} years depending on the assumed decay mode are established. It is seen that the muon neutrino serves as a major source of background in the present nucleon lifetime experiment. In future experiments, where it is possible to positively identify all muon neutrino events, improved lifetime limits may be established.

APPENDIX I. NUCLEON DECAY COUNTING RATE IN A THIN* FLAT DETECTOR.

In the following derivations it is assumed that; 1) the materials of the cavity walls (rock), the active detector material (scintillator), and the detector covers (lucite, press-wood and sheet steel) were homogeneous;
2) the decay products are emitted isotropically; and
3) the lifetime of the nucleon is independent of the nucleus to which it is bound.

A) Nucleons in the Detector (One Ionizing Decay Fragment).

In order to discriminate against natural radioactivity a minimum detection threshold $E_T \simeq 10$ MeV was selected. Since nucleon decay fragments near their origin are minimum ionizing, the path-length m to deposit the threshold energy E_T is

$$m = \frac{E_T}{\frac{(dE)}{(dx)}}$$

---

* The detector is here assumed to be so thin that the fraction of particles cutting corners is negligible. In the final results, Appendix III, a correction for corner cutting is included.

where $\frac{dE}{dx}$ is the rate of energy loss with distance in the detector medium. An ionizing fragment leaving a thin detector at an angle α to the detector normal and originating a distance greater than $m\cos\alpha$ from the detector edge will be counted. See Fig. 12. For a thin slab the rate of detected single ionizing decay fragments emitted at angle α within solid angle $d\Omega$ is

$$d^2\left(\frac{\Delta N}{\Delta t}\right) = \frac{dn}{dt_d} \frac{A(t + s - m\cos\alpha)}{4\pi} d\Omega \qquad (3)$$

where

n_d = number of nucleons per unit volume in the detector.

$\frac{dn}{dt_d} \simeq \frac{n_d}{\tau}$ = nucleon decay rate per unit volume in the detector.

τ = nucleon mean life.

A = Area of detector.

t = thickness of active detector material (scintillator).

$s = \frac{\Sigma P_i x_i}{P_d}$ = effective thickness of detector walls (plastic tank walls plus cover)*

---

* The plastic tank is similar in composition and chemical make-up to the scintillator, and therefore, its presence is most easily included as part of the scintillation volume. Other parts of the detector cover are negligible but for completeness their effect is lumped into the detector wall thickness.

P_i = density of various materials in detector walls.

x_i = thickness of various detector walls.

P_d = density of active detector material.

The single ionizing decay fragment counting rate from decays in the detector is therefore

$$\frac{\Delta N}{\Delta t} = \frac{n_d}{\tau_1} \int_{\Omega} \left(\frac{A\cos\alpha}{4\pi}\right) \left((t+s)/\cos\alpha - m\right) d\Omega = \frac{n_d}{\tau_1} V_{eff} \qquad (4)$$

B) Nucleons in the Detector (Two Ionizing Decay Fragments)

If two ionizing fragments are emitted, at least one of the fragments will always be detected because the fragments proceed in opposite directions. The two-ionizing fragment counting rate for decays in the detector is therefore

$$\frac{\Delta N}{\Delta t} = \frac{n_d}{\tau_2} V_{detector} \qquad (5)$$

C) Nucleons Outside the Detector (Single Ionizing Decay Fragment).

As seen from Fig. 13 the nucleon decay detection rate for a single ionizing fragment emitted in area dA from volume dV is

$$d^5\left(\frac{\Delta N}{\Delta t}\right) = \frac{dA \cos\alpha}{4\pi r^2} \frac{dn_W}{dt} dV \qquad (6)$$

where

n_W = number of nucleons per unit volume in cavity wall.

r = distance from dA to dV.

r_o = distance from dA to cavity wall.

$\frac{dn_W}{dt} \simeq \frac{n_W}{\tau_1}$ = nucleon decay rate per unit volume wall.

R_W = total range of decay fragment in wall.

If the source volume dV is not deep within the cavity wall, the fragment can emerge from the wall and be detected. Since a particle is heavily ionizing at the end of its range, a particle just reaching the detector need only have a negligible fraction of its range within the detector to deposit the required threshold energy. Thus to a very good approximation the effective volumes extend into the wall <u>along r</u> to a depth equal to the range of the decay fragment.* The counting rate due to single ionizing fragment nucleon decay in the wall is therefore

---

* If the energy necessary to penetrate the detector walls is not small compared to the initial fragment energy, a correction is necessary.

$$\frac{\Delta N}{\Delta t} = \frac{n_W}{\tau_1} \int_A \int_\Omega \int_{r_o}^{r_o+R_W} \left(\frac{dA \cos\alpha}{4\pi}\right) d\Omega \, dr \qquad (7)$$

If the detector is in a cavity of wall thickness greater than R_W the integral over $\underline{r}$ may be trivially performed. Note that the result does not depend upon the distance r_o from the cavity wall to any detector element. For rectangular detectors, the area integral may be determined by inspection. Hence,

$$\frac{\Delta N}{\Delta t} = \frac{R_W n_W}{\tau_1} \int_\Omega \left(\frac{A \cos\alpha}{4\pi}\right) d\Omega = \frac{R_W n_W}{\tau_1} A_{eff} \qquad (8)$$

D) Nucleons outside Detector (Two Ionizing Decay Fragments).

The decay fragments proceed in opposite directions so that the counting rate for both fragments is the sum of two terms identical to Equation (8), a term for each fragment.

E) Summary.

The mean lifetimes for single ionizing fragment nucleon decay and two ionizing fragment nucleon decay are respectively:

$$\tau_1 = \frac{1}{\frac{(\Delta N)}{(\Delta t)}} \left(n_d V_{eff} + n_w R_w A_{eff} \right) \qquad (9)$$

$$\tau_2 = \frac{1}{\frac{(\Delta N)}{(\Delta t)}} \left(n_d V_{detector} + n_w R'_w A_{eff} + n_w R''_w A_{eff} \right) \qquad (10)$$

APPENDIX II. NUCLEON DECAY COINCIDENCE COUNTING RATE IN TWO THIN FLAT PARALLEL DETECTORS.

A) Single Ionizing Decay Fragment.

The calculation of the counting rate proceeds from the application of the equations derived in Appendix I. Equations (4) and (8) give the coincidence rate if the area A is replaced by $A(\alpha,\beta)$, the area of the detector (Fig. 14) or of the cavity wall (Fig. 15) within which a nucleon decay fragment in direction* (α,β), within solid angle $d\Omega$, will pass through both detectors. This is the area of overlap or "shadow area" of the two detectors in the direction (α,β). The effective volumes extend along r into the rock a distance equal to $(R_W - R(E)_W)$ where E is the energy necessary to penetrate the first detector and reach the second. In this case Equations (4) and (8) become

$$\frac{\Delta N}{\Delta t} = \frac{n_d}{\tau_1} \int_{\Omega} \frac{A(\alpha,\beta)\cos\alpha}{4\pi} \left((t + s)/\cos\alpha - m\right) d\Omega \qquad (11)$$

$$\frac{\Delta N}{\Delta t} = \frac{n_W}{\tau_1} \int_{\Omega} \frac{A(\alpha,\beta)\cos\alpha\ (R_W - R(E)_W)}{4\pi} d\Omega \qquad (12)$$

where

---

* See Fig. 16 for definition of α and β.

$A(\alpha,\beta)$ = area of shadow on one detector cast by parallel rays in the direction (α,β) from the other detector.

R_W = total range of decay fragment in rock (cm).

$R(E)_W$ = range of decay fragment of energy E in rock (cm).

E = energy necessary for a fragment travelling in direction (α,β) to penetrate the first detector and just reach the active region of the second.

At those angles $\alpha \leq \alpha_o$ where $(R_W - R(E)_W) \leq 0$, the integrand in Equation 12 is zero. At $\alpha=\alpha_o$, the function $((t + s)/\cos\alpha - m)$ in Equation 11 changes to R_d (range of the fragment in the detector)*. The integrands may be considered to be valid for all angles if the roles of the two detectors are reversed as the angle α passes to values greater than $\pi/2$. Equation (12) is simplified by the approximation that the range of an ionizing particle is inversely proportional to the density of the stopping medium and that for a wide variation of energy the ranges of a particle in two different materials are proportional. (See Appendix IV.) Therefore,

---

* Since in most cases $R_d >> (t + 3s)$ it is sufficiently accurate to terminate Equations (11) and (12) at $\alpha=\alpha_o$.

$$n_w R(E)_w \cong k n_d R(E)_d = k n_d \frac{(3s + t)}{\cos\alpha} \qquad (13)$$

where k has a value near unity. Equation (12) becomes

$$\frac{\Delta N}{\Delta t} = \frac{1}{\tau_1} \int_{\substack{\Omega \\ \alpha<\alpha_o}} \frac{A(\alpha,\beta)\cos\alpha}{4\pi} \left(n_w R_w - \frac{k n_d (t+3s)}{\cos\alpha}\right) d\Omega \qquad (14)$$

Adding (11) to (14) the total counting rate from nucleons inside and outside the detector is

$$\frac{\Delta N}{\Delta t} = \frac{1}{\tau_1} \int_{\substack{\Omega \\ \alpha<\alpha_o}} \frac{A(\alpha,\beta)\cos\alpha}{4\pi} \left(n_w R_w + \frac{n_d (t+s)(1-k)}{\cos\alpha} - \right.$$

$$\left. - \frac{2k n_d s}{\cos\alpha} - m n_d\right) d\Omega \qquad (15)$$

$$= \frac{\left(-2k n_d s - n_d (t+s)(k-1)\right)}{4\pi\tau_1} \int_{\substack{\Omega \\ \alpha<\alpha_o}} A(\alpha,\beta)\, d\Omega +$$

$$+ \frac{(n_w R_w - m n_d)}{4\pi\tau_1} \int_{\substack{\Omega \\ \alpha<\alpha_o}} A(\alpha,\beta)\cos\alpha\, d\Omega \qquad (16)$$

$$= \frac{(n_w R_w - m n_d)}{4\pi\tau_1} A_p - \frac{\left(n_d (t+s)(k-1) + 2k n_d s\right)}{4\pi\tau_1} B_p \qquad (17)$$

where the following integrals have been defined,

$$A_p = \int_{\substack{\Omega \\ \alpha<\alpha_o}} A(\alpha,\beta)\cos\alpha \, d\Omega \quad = \text{aperture.} \tag{18}$$

$$B_p = \int_{\substack{\Omega \\ \alpha<\alpha_o}} A(\alpha,\beta) \, d\Omega \quad = \text{"pseudo aperture".} \tag{19}$$

B) Two Ionizing Fragments.

For nucleons inside the detector the decay fragments emitted in direction (α,β) and depositing energy greater than the threshold energy may originate anywhere along r within either detector. Hence the counting rate for nucleons inside and outside the detector is given by the sum of two terms (one for each fragment) identical to equation (17) with m = o. Each integral can in most cases be accurately terminated at the angle α at which one of the fragments can not penetrate the full depth of one detector.

C) Approximate Formulae for Lifetimes from Coincidence Counting Rates.

The lifetime results given in this thesis were calculated from equation (17). However for purposes of discussion the approximate nucleon coincidence counting rate relations derived below are useful.

In the detector of the present experiment mn_d and sn_d are small compared to $n_w R_w$ and k is approximately 1. Hence from Equation (17) and discussion in B) above, the nucleon mean lifetimes for single ionizing fragment and two ionizing fragment nucleon decay are respectively

$$\tau_1 \simeq \frac{1}{\frac{(\Delta N)}{(\Delta t)}} \frac{R_w n_w}{4\pi} A_p \qquad (20)$$

$$\tau_2 \simeq \frac{1}{\frac{(\Delta N)}{(\Delta t)}} \frac{(R'_w + R''_w) n_w}{4\pi} A_p \qquad (21)$$

APPENDIX III. COINCIDENCE APERTURE FOR LONG NARROW THIN FLAT DISCONTINUOUS PARALLEL DETECTORS.

In this appendix the aperture A_p is particularised to the case of coincidences between two sides of an array of long parallel detectors called a rail geometry. The calculation of pseudo aperture B_p follows almost the same steps and will not be given here. As noted earlier it is convenient to group the individual detectors into discontinuous rails and further group the various pairs of rails into the three classes shown in Figs. 6, 7 and 8.

Formulae for the aperture of the identical pairs of each class are now developed. The apertures are most easily calculated using the polar co-ordinates (ϕ,ξ),* shown in Figs. 16 and 17. In this co-ordinate system the aperture is**

---

* Equation (22) in no way depends on the location of the origin of the co-ordinate system relative to the detector, but for other reasons it is convenient to visualise the origin as located at the geometric centre of the detector array.

** In the following discussion the integrals are all terminated at angles ξ_o and ϕ_o which are equivalent to α_o.

$$A_p = \int_{\Omega} A(\alpha,\beta)\cos\alpha \, d\Omega =$$

$$= \int_{\phi=0}^{2\pi} \int_{\xi=-\pi/2}^{\pi/2} A(\phi,\xi)(\cos\xi\cos\phi)\cos\xi \, d\xi d\phi \qquad (22)$$

where $A(\phi,\xi)$ vanishes for certain angles corresponding to directions in which it is not possible to pass a particle through the sensitive regions of both sides of the array.

Since both sides of the detector array are identical and are directly opposite each other, the configuration is symmetric about the three mutually perpendicular planes defined by $\phi=o$, $\phi=\pi/2$, and $\xi=o$. Hence

$$A_p = 8 \int_{\phi=o}^{\pi/2} \int_{\xi=o}^{\pi/2} A(\phi,\xi)(\cos^2\xi\cos\phi) \, d\xi d\phi \qquad (23)$$

For flat parallel rectangular detectors $A(\phi,\xi)$ is the product of the length and the height of the rectangular "shadow area" and is

$$A(\phi,o) = H(\phi,\xi)\, L(\phi,\xi) \qquad (24)$$

The boundaries of the shadow area are given by the envelope of parallel rays in direction (ϕ,ξ) having path-length in each detector greater than the threshold path-length m as defined in Appendix I.

The height of the shadow $H(\phi,\xi)$ is determined by inspection from Figs. 18 and 19. The distance $m\cos\xi$ is the threshold path-length projected into a plane perpendicular to the rails. The length of the shadow $L(\phi,\xi)$ is determined by inspection from Fig. 20 where the plane of the figure is a cross-section of the detector at any given angle ϕ. The length of the shadow gaps $G(\phi,\xi)$ is given in Fig. 21 and 22. In the expression $L(\phi,\xi)$, the term ℓ is much greater than any other term and the value of $1/\cos\phi$ does not change greatly over the entire range of ϕ for any one class. Thus with good accuracy $L(\phi,\xi) \cong L(\phi_c,\xi)$ where ϕ_c is the angle of the central ray for each class (see Fig. 24). Hence

$$A_p = 8 \int_{\xi=0}^{\pi/2} L(\phi_c,\xi) \left(\int_{\phi=0}^{\pi/2} H(\phi,\xi)\cos\phi d\phi \right) \cos^2\xi d\xi \quad (25)$$

where it is convenient to define

$$H_p(\xi) = \int_{\phi=o}^{\pi/2} H(\phi,\xi)\cos\phi d\phi$$

Using the values of $H(\phi,\xi)$ determined from Figs. 18 and 19,

$$H_p = \int_{\phi=o}^{\phi_n} 0 + \int_{\phi=\phi_m}^{\pi/2} 0 +$$

$$+ \int_{\phi=\phi_n}^{\phi_c} \left((t+d)\sin\phi - (c-h)\cos\phi - 2m\cos\xi\sin\phi\cos\phi\right)d\phi +$$

$$+ \int_{\phi=\phi_c}^{\phi_m} \left((h+c)\cos\phi - (d-t)\sin\phi - 2m\cos\xi\sin\phi\cos\phi\right)d\phi \qquad (26)$$

where $\phi_n(\xi)$ and $\phi_m(\xi)$ are defined by the angles at which their respective integrands vanish (See Figs. 25 and 26). Hence

$$H_p(\xi) = -2d\cos\phi_c - 2c\sin\phi_c + m\cos\xi(\sin^2\phi_m - \sin^2\phi_n) +$$

$$+(d-t)\cos\phi_m + (h+c)\sin\phi_m - 2m\cos\xi\sin^2\phi_m +$$

$$+(t+d)\cos\phi_n + (c-h)\sin\phi_n + 2m\cos\xi\sin^2\phi_n \qquad (27)$$

From Figs. 24, 25 and 26, it is seen that

$$H_p(\xi) = E + F - 2D + m\cos\xi(\sin^2\phi_m - \sin^2\phi_n). \qquad (28)$$

To facilitate calculation it is convenient to reformulate the above equation in terms of the angles ε and ζ defined in Figs. 27 and 28.

$$\begin{aligned} H_p(\xi) = {} & E-(D+S-2m\cos\xi\sin\phi_m\sin\phi_c)-2m\cos\xi\sin\phi_m\sin\phi_c+ \\ & + m\cos\xi\sin^2\phi_c + \\ & + F-(D-S+2m\cos\xi\sin\phi_n\sin\phi_c) + 2m\cos\xi\sin\phi_n\sin\phi_c- \\ & - m\cos\xi\sin^2\phi_c+ \\ & + m\cos\xi(\sin\phi^2_m - \sin^2\phi_n) \end{aligned} \qquad (29)$$

$$\begin{aligned} H_p(\xi) = {} & E(1-\cos\varepsilon) + F(1-\cos\zeta)+ \\ \text{Class II\&III} \quad & + m\cos\xi(\sin(\varepsilon+\phi_c)-\sin\phi_c)^2 - \\ & - m\cos\xi(\sin\phi_c-\sin(\phi_c-\zeta))^2 \end{aligned} \qquad (30)$$

Since H_p includes only directions in which $\phi>0$, the H_p for Class I is simply derived from equation (26) with $\zeta=\phi_c=0$. Hence equation (30) becomes

$H_p = E(1-\cos\varepsilon) + m\cos\xi\sin^2\varepsilon$ where

Class I

$$\varepsilon = \phi_m = \tan^{-1}\left(\frac{h-2m\cos\xi\sin\varepsilon}{(d-t)}\right) \qquad (31)$$

Class I

The variation of $H_p(\xi)$ with ξ is small. In Class III, where $H_p(\xi)$ has the greatest variation, $H_p(\xi)$ has the relative values of 1.00, 1.09 and 1.25 for respectively $\xi=0^\circ$, 54° and 90°. Since 90% of the aperture is contained within angles less than $\xi=54^\circ$, the conservative approximation that $H_p=H_p(0)$ is used. Hence

$$A_p = 8H_p \int_{\xi=o}^{\pi/2} L(\phi_c\xi)\cos^2\xi \, d\xi = 8H_pL_p \qquad (32)$$

where from Fig. 20

$$L_p = \int_o^{\xi_d} \left(\ell - (d-t)\tan\xi/\cos\phi_c - 2m\sin\xi\right)\cos^2\xi \, d\xi +$$

$$+ \int_{\xi=\xi_d}^{\pi/2} 0 - \int_{\xi=o}^{\pi/2} G(\phi_c\xi)\cos^2\xi \, d\xi \qquad (33)$$

Because the detectors are very long ξ_d has a value very near $\pi/2$. As a consequence the first integrand in Equation (33) is very small for $\xi>\xi_d$ and L_p is accurately given by

$$L_p \simeq \int_{\xi=o}^{\pi/2} (\ell - (d-t)\tan\xi/\cos\phi_c - 2m\sin\xi)\cos^2\xi \, d\xi - G_p \quad (34)$$

$$L_p = \frac{\ell\pi}{4} - \frac{(d-t)}{2\cos\phi_c} - \frac{2m}{3} - G_p \quad (35)$$

where the quantity G_p is

$$G_p = \int_{o}^{\pi/2} G(\phi_c\xi)\cos^2\xi \, d\xi \quad (36)$$

From Figs. 21, 22 and 23 it is seen that G_p

$$= (Q-1)\int_{o}^{\xi_g} G_1\cos^2\xi \, d\xi + 2(Q-1)\int_{\xi_g}^{\xi_t} G_2\cos^2\xi \, d\xi + \int_{\xi_t}^{\pi/2} 0 \quad (37)$$

$$\begin{aligned}
&= \int_{o}^{\xi_g} \{2(Q-1)\{g-(t/\cos\phi_c)\tan\xi+2m\sin\xi)+ \\
&+(Q-1)(-g+(t/\cos\phi_c)\tan\xi-2m\sin\xi+(d/\cos\phi_c)\tan\xi)\}\cos^2\xi \, d\xi \\
&+\int_{\xi_g}^{\xi_t} 2(Q-1)(g-(t/\cos\phi_c)\tan\xi+2m\sin\xi)\cos^2\xi \, d\xi \\
&= \int_{o}^{\xi_t} 2(Q-1)(g-(t/\cos\phi_c)\tan\xi+2m\sin\xi)\cos^2\xi \, d\xi + \\
&+\int_{o}^{\xi_g} (Q-1)(-g+(d+t)\tan\xi/\cos\phi_c-2m\sin\xi)\cos^2\xi \, d\xi
\end{aligned} \quad (38)$$

$$G_p = 2(Q-1)\left\{g\left(\frac{\xi_t}{2} + \frac{\sin 2\xi_t}{4}\right) - (t/\cos\phi_c)\left(\frac{\sin^2\xi_t}{2}\right) + \right. \tag{39}$$

$$\left. + \frac{2m}{3}(1-\cos^3\xi_t)\right\} + (Q-1)\left\{-g\left(\frac{\xi_g}{2} + \frac{\sin 2\xi_g}{4}\right) + \right.$$

$$\left. + \frac{(d+t)\sin^2\xi_g}{2\cos\phi_c} - \frac{2m}{3}(1-\cos^3\xi_g)\right\}$$

SUMMARY.

The aperture for the individual pairs of discontinuous rail detectors has been calculated above. The total aperture for all pairs in each class is

$$A_{p_I} = 3(8H_{p_I} L_{p_I}) \tag{40}$$

$$A_{p_{II}} = 2(8H_{p_{II}} L_{p_{II}}) \tag{41}$$

$$A_{p_{III}} = 1(8H_{p_{III}} L_{p_{III}}) \tag{42}$$

where

$$H_{p_{II\&III}} = E(1-\cos\varepsilon)+F(1-\cos\zeta)+m\left(\sin(\varepsilon+\phi_c)-\sin\phi_c\right)^2 - \tag{43}$$

$$- m\left(\sin\phi_c-\sin(\phi_c-\zeta)\right)^2$$

$$H_{p_I} = E(1-\cos\varepsilon)+m(\sin\varepsilon) \tag{44}$$

$$L_{p_{I,II\&III}} = \frac{\ell\pi}{4} - \frac{(d-t)}{\cos\phi_c} - \frac{2m}{3} - G_p(\phi_c) \tag{45}$$

APPENDIX IV. NUCLEON DECAY FRAGMENT RANGES.

The material of the cavity walls was assumed to be all S_iO_2, since rock contained ~ 90% silicon dioxide and the other materials (alumina, soda, potash and iron) had a Z/A close to that of S_iO_2. The scintillation material of the detector had the approximate formula $CH_{1.8}$. This same chemical composition, with a density correction, was assigned to the material of the detector walls (lucite, press-wood, and a minor amount of sheet iron). The ranges for the various nucleon decay fragments are calculated from the following formulas and the results listed in Table IX.

The range of μ, π and k decay fragments was computed from an interpolation formula for various materials developed by Sternheimer[12]. The formula is a power law fit to the ranges of a proton in Be, C, Al, Cu, and Pb computed from the Bethe-Block formula[13] and is

$$R(E) = R(2MeV) + \tag{46}$$
$$+ \frac{A}{2Z}\left(\Phi(E_p)\frac{m_i}{m_p}\right)(1 + G_1x + G_2x^2 + G_3x^3)$$

where $x = \log_{10}\left(\frac{I}{I_{Al}}\right)$

I = mean excitation and ionization potential for medium under consideration.

I_{Al} = mean excitation and ionization potential for Aluminium.

A = Atomic weight.

Z = Atomic number.

$\phi(E_p)$ = Range of proton in Aluminium (tabular entry as function of E_p).

E = Energy of particle under consideration.

E_p = Equivalent energy of proton = $(E\frac{m_p}{m_i})$

m_i = rest mass of particle under consideration.

m_p = rest mass of proton.

G_i = constants of power law expansion (tabular entry as function of E_p).

The mean excitation and ionization potential for the rock and scintillator, which contained more than one atomic variety, was derived with the Bragg rule (Equation 1.1.24 reference 13).

$$\log_{10}\bar{I} = \sum_i f_i \log_{10} I_i \qquad (47)$$

where

$$f_i = \frac{n_i Z_i}{\sum_i n_i Z_i}$$

n_i = number of atoms of given variety per molecule.

Z_i = atomic number of given variety.

I_i = mean excitation and ionization potential of material of given variety.

The value of I_i, where not directly available, was scaled by the ratio of atomic number from substances of similar atomic number. A correction for the nuclear absorption of the π nucleon decay fragment was made assuming an attenuation length of $120 g/cm^2$.

The ranges of electrons were computed from a formula, based on a Monte Carlo calculation of Wilson[14]. This formula,

$$R(E) = X_o \ln 2 \ln\left(\frac{E}{E_c \ln 2} + 1\right) \qquad (48)$$

E = initial electron energy.

X_o = radiation length for material under consideration.

E_c = critical energy for material under consideration.

gives the range of the initial electron and not its subsequent products. The radiation length was computed from Equation (1.1.67) of reference 13 which is

$$\frac{1}{X_o} = \frac{4N_o}{A} Z(Z+1.3)(5.79\times10^{-28}\,cm^2) \ln\left(183\, Z^{-\frac{1}{3}}\right) \quad (49)$$

N_o = Avogadros Number.

A = Atomic weight.

Z = Atomic number.

The critical energy for SiO_2 was assumed to be the same as that for Al. The critical energy for the scintillator was taken as that for carbon increased by a factor of 1.3 to correct for the ratio of ionization loss of scintillator relative to carbon.

The nucleon decay γ-rays are assumed to convert (by pair production) one half of their energy to at least one electron which then has a range as discussed above. Since <u>all</u> of the γ-rays in the rock are so converted the density of such conversions, which send electrons towards the detector from the wall of the tunnel, is identically the same as the nucleon decay density. The contribution of γ-rays which originate from decays in the detector is ignored.

APPENDIX V. LIGHT PULSER.

A large multidetector system must have a quick and easy method for testing the correct operation of all of its components. The test should on command produce an event in each detector and require that it be detected and recorded exactly as an actual event, thus testing each and every component under actual operating conditions.

In the Case-Wits Neutrino Experiment a radioactive source was used to energy calibrate the detectors and partially test parts of the system, but since the detectors were designed to operate on a minimum deposited energy of ~10 MeV, the energy from any practical radioactive source was not great enough for an adequate test. Due to the deep underground location, cosmic ray muons were too infrequent to be useful. A suitable source was found in an ultraviolet light pulser which was used to simulate scintillation events for test purposes.

ULTRAVIOLET TESTING OF SCINTILLATORS.

In a scintillator there are many different "channels" by which the complex of excited states left

behind by a penetrating charged particle may return to the ground state. The most interesting channels from our point of view are those intermolecular channels which transfer excitation energy from non-fluorescing molecules to fluorescing molecules. These channels are in competition with other channels which de-excite by non-radiative processes (i.e. quenching). Ultraviolet photons of energy greater than that of the scintillator fluorescent transition, can excite many of the lower energy levels which are excited directly or indirectly by penetrating particles. Although it is not possible to say exactly at what stage in the de-excitation process the ultraviolet excitation and scintillation channels become the same, they are similar at those energy levels which are directly excited by the ultraviolet radiation and exactly the same at the visible fluoresence transition since it is the only channel which leads to a scintillation detector response. The ultraviolet conversion efficiency should therefore directly reflect any changes in scintillation efficiency caused by agents which introduce non-radiative transitions of energy less than that of the

ultraviolet photons.

It should be noted that the most crucial steps in the scintillation process occur after the fluorescent transition where the light must undergo a multitude of absorbtions, re-emissions, and slight (downward) energy shifts in order to escape the "resonance trap" within which it was created. Any slight loss here or in the subsequent transmission to the phototubes can drastically reduce the scintillation efficiency. In addition to testing the scintillator efficiency, ultraviolet light also makes a very good way of measuring the response versus position of a scintillation detector.

LIGHT PULSE GENERATOR.

A scintillation event is the result of almost instantaneous excitation by the passing charged particle. The ultraviolet light must duplicate this very quick excitation in order to test the pulse electronics of a scintillation system. The ultraviolet pulse need only be shorter than the overall scintillation detector response time, which in most cases is limited by the detector electronics.

The light pulser unit was very similar to that described by Kerns[15]. A Schott UG-11[16] glass filter was used to select the ultraviolet light (3800 to 2900 Å) from a P.E.K. 118 hydrogen corona lamp[17] and pass it through the lucite* walls of the scintillation tank to the scintillator fluid. The lamp was flashed with a short duration electrical pulse derived by discharging a 25 pf capacitor, charged to 2000 volts through an 82 ohm resistor in parallel with the lamp. The charged capacitor was switched to the lamp with a mercury wetted contact relay.[18] In the early phase of the experiment a manual unit was carried to each detector element. Later an automatic sequencing unit was used to pulse a lamp fixed on each detector element. A complete detector system test was carried out before and after each 35 hour run. After the automatic unit was installed two additional test sequences were performed during a 35 hour run.

---

* Transmission of a 3/8 inch thick sample of an ultraviolet non-absorbing lucite is reduced to ~40% at 3000 Å.

REFERENCES.

1. E.C.G. Stückelberg, Helv. Phys. Acta. 11, 225, 229 (1938).

2. E.P. Wigner, Proc. Am. Phil. Soc. 93, 521 (1949); Proc. Natl. Acad. Sci. U.S. 38, 449 (1952).

3. M. Goldhaber (footnote in reference 4).

4. F. Reines, C.L. Cowan, Jr., and M. Goldhaber, Phys. Rev. 96, 1157 (1954).

5. F. Reines, C.L. Cowan, Jr., and H.W. Kruse, Phys. Rev. 109, 609 (1957).

6. G.K. Backenstoss, H. Frauenfelder, B.D. Hyams, L.J. Koester, Jr., and P.C. Marin, Nuovo cimento 16, 749 (1960).

7. C.C. Giamati and F. Reines, Phys. Rev. 126, 2178 (1962).

8. W.R. Kropp and F. Reines, Phys. Rev. 137, 740 (1965).

9. F. Dix and F. Reines (Private communication 1966).

10. F. Reines, M.F. Crouch, H.S. Gurr, T.L. Jenkins, W.R. Kropp, G.R. Smith, B.S. Meyer, and J.P.F. Sellschop, Phys. Rev. Letters 15, 429 (1965); see also the papers by members of the Case-Wits Group at The Scintillation Symposium, Washington D.C. (1966).

11. Proceedings of the International Conference on Weak Interactions, Argone National Laboratory, ANL - 7130 (1966).

12. R.M. Sternheimer, Phys. Rev. 118, 1045 (1960).

13. R.M. Sternheimer, in Methods of Experimental Physics, Vol. 5, Part A, Edited by L.C.L. Yuan and C.Wu, Academic Press, New York, (1961), Chap. 1. p 4.

14. R.R. Wilson, Phys. Rev. 84, 100 (1951). (See also reference 13, p.62).

15. Q.A. Kerns in Proceedings of An International Conference on Cosmic Rays pp. 64-66, Interscience Publishers, New York, 1961.

16. Fish-Schurman Corporation, 70 Portman Road, New Rochelle, N.Y.

17. P.E.K. Laboratories, 825 E, Evelyn, Sunnyvale, California.

18. C.P. Clare and Co., 3101 Pratt Blvd. Chicago 45, Illinois.

TABLE I. SUMMARY OF NUCLEON LIFETIME EXPERIMENTS.

Experimenters	Nucleon Lifetime (Years)	Nucleon Decay Detection Method	Notes
Goldhaber[3] (1954)	1.4×10^{18}	Spontaneous fission of Th^{232} after excitation by nucleon decay.	This assumes that the rearrangement energy upon loss of a nucleon is sufficient to cause fission of the residual nucleus.
Reines[4] Cowan Goldhaber (1954)	1×10^{22}	High energy decay fragment. Liquid scintillation, 30 m below surface.	Toluene in detector and paraffin outside detector as source of nucleons.
Reines[5] Cowan Kruse (1957)	4×10^{23}	Proton decay in deuteron. High energy fragment plus neutron left over from deuteron after decay of proton. Delayed coincidence and liquid scintillation, 61 m below surface.	
Backenstoss[6] Frauenfelder Hyms Koester Marin (1960)	2.8×10^{26}	High energy fragment; upward going particles. Čerenkov and scintillation, 800 m below surface.	At least 250 MeV assumed to be available to decay particle. Water, lead, and rock as source of nucleons. Result based on combined measurements for neutrons and protons.

TABLE I. SUMMARY OF NUCLEON LIFETIME EXPERIMENTS. (Continued)

Experimenters	Nucleon Lifetime (Years)	Nucleon Decay Detection Method	Notes
Giamati[7] Reines (1962)	1×10^{26} to 7×10^{27} Depending on mode.	High Energy fragment. Liquid scintillation with anticoincidence shield, 585 m below surface.	Decalin in detector and iron outside detector as source of nucleons.
Kropp[8] Reines (1964)	5×10^{27} to 4×10^{28} Depending on mode.	High energy fragment. Liquid scintillation with anticoincidence shield, 585 m below surface.	Decalin in detector and iron outside detector as source of nucleons.
Dix[9] Reines.	In Progress.	Neutron left over from deuteron after decay of proton. Not dependant on decay mode.	- - - -
Present Experiment.	2×10^{28} to 8×10^{29} Depending on mode.	High energy fragment. Liquid scintillation, 3200 m below surface. Horizontal going particles.	- - - -

TABLE II. ASSUMED TWO BODY MODES OF NUCLEON DECAY.

Nucleon	Fragment 1	Kinetic Energy (MeV)		Fragment 2	Kinetic Energy (MeV)
p	π^+	340	+	ν	458
p	k^+	105		ν	339
p	e^+	469		γ	469
p	μ^+	369		γ	464
n	π^+	340	+	e^-	458
n	μ^+	239		k^-	100

TABLE III. EVENTS INVOLVING TWO DETECTOR ELEMENTS ONE ON EACH SIDE OF THE DETECTOR ARRAY. PERIOD OF OBSERVATION 27 OCTOBER, 1964 TO 1 APRIL, 1966.

Class	Time (h) Greenwich	Date	Angle to Detector Normal (ξ)(deg).	Mean Distance from North End of Detector (meter)	Energy Deposited (MeV)	
					East	West
I	2148	23 Feb 65	+ 21°	20.6	29	18
II	0020	1 Mar 65	+ 68°	26.7	55	118
I	1852	17 Mar 65	- 46°	19.1	19	16
I	1416	20 Apr 65	- 34°	6.1	23	24
I	2237	1 Jun 65	- 70°	5.8	18	18
II	0142	3 Jun 65	+ 20°	18.8	5	18
II	1521	1 Jul 65	+ 41°	13.0	21	30
I	1406	21 Nov 65	~- 40	~20.7	~40	25
I	1642	7 Dec 65	+ 3°	19.5	38	23
I	0615	25 Dec 65	- 15°	27.6	20	20
II	0047	30 Dec 65	- 65°	50.8	21	13
I	0304	28 Feb 66	- 42°	46.1	18	18

TABLE IV. NUMBER OF EVENTS INVOLVING ELEMENTS ON ONE SIDE OF THE DETECTOR ARRAY. PERIOD OF OBSERVATION 27 OCTOBER, 1964 TO 1 APRIL, 1966.

Class	Number of Events
VI*	3
V	30
IV	119

* Class VI events are restricted to those in which the deposited energy in each detector element is greater than 20 MeV.

TABLE V. OBSERVED EVENTS CONSISTANT WITH NUCLEON DECAY COMPARED TO APERTURE - RUN TIME PRODUCT. PERIOD OF OBSERVATION 27 OCTOBER 1964 TO 1 APRIL 1966.

Class	Aperture Bays 1 to 6 cm^2 ster x 10^4	Aperture Bays 7 to 9 cm^2 ster x 10^4	Total Aperture x Run Time cm^2 ster sec x 10^{11}	Number of Events*	Intensity cm^{-2} ster^{-1} sec^{-1} x 10^{-12}
VI	2.7	1.05	7.5	3	4.0
V	15.8	6.11	43	30	6.9
IV	595	257	1650	119	0.72
III	17.0	6.5	46	1*	0.22
II	52.2	20.2	143	4	0.28
I	47.6	18.5	130	8	0.61

* Since no events have been observed in Class III, the number of observed events is taken as one in estimating lifetime limits.

TABLE VI. LOWER LIMITS ON NUCLEON LIFETIMES FOR SPECIFIED DECAY MODES. UNITS OF 10^{28} YEARS.

Assumed Decay Mode	FREE PROTONS		ALL NUCLEONS	
	Background Not Subtracted	Background Subtracted	Background Not Subtracted	Background Subtracted
$p \rightarrow \pi^+ + \nu$	.8	1.2	9	17
$p \rightarrow k^+ + \nu$	.3	.6	1	2
$p \rightarrow e^+ + \gamma$	.9	1.3	16	30
$p \rightarrow \mu^+ + \gamma$	.9	1.3	49	82
$n \rightarrow \pi^+ + e^-$	-	-	21	36
$n \rightarrow \mu^+ + k^-$	-	-	25	49

TABLE VII. DIMENSIONS OF DETECTOR ARRAY.

Symbol	Bays 1 to 6	Bays 7 to 9	Definition
ℓ	3577 cm.	1686 cm.	total length of rail including gaps.
g	59 cm.	133 cm.	length between sensitive regions of detectors in given rail.
i	14.3 cm.	14.3 cm.	height between sensitive regions of detector elements.
v	547 cm.	473 cm.	length of sensitive region of detector element.
h	56 cm.	56 cm.	height of sensitive region of detector element.
t	12.7 cm.	12.7 cm.	thickness of sensitive region of detector element.
s	1.6 cm.	1.6 cm.	effective thickness of detector walls.
d	180 cm.	180 cm.	horizontal distance, centre to centre, between sides of detector.
Q	6	3	number of detector elements in given rail.

TABLE VIII. DETECTOR ARRAY DERIVED QUANTITIES.

Bays	Symbol	Units	Class I	Class II	Class III	Definition
1 to 9	ϕ_c	deg.	0	21.3	38.0	central angles of ϕ
1 to 9	ε	deg.	17.3	14.1	10.3	$\phi_c+\varepsilon = \phi_m$ max angle of ϕ
1 to 9	ζ	deg.	0	16.7	13.0	$\phi_c-\zeta = \phi_n$ min angle of ϕ
1 to 9	c	cm.	0	70.5	141	vertical distance between like points on detectors on opposite sides of the array.
1 to 9	D	cm.	180	194	229	"ϕ_c Distance"
1 to 9	E	cm.	176	206	251	"ϕ_m Distance"
1 to 9	F	cm.	-	194	213	"ϕ_n Distance"
1 to 9	$\bar{\theta}_c$	deg.	90	72	59	mean zenith angle (vertical)
1 to 9	w	unity	3	2	1	number of identical rail pairs in a given class.
1 to 9	H_p	cm.rad	25.6	27.9	9.39	aperture height.

TABLE VIII. DETECTOR ARRAY DERIVED QUANTITIES. (Continued)

Bays	Symbol	Units	Class I	Class II	Class III	Definition
1 to 6	L_p	$\frac{\text{cm ster}}{\text{rad}}$	2327	2321	2305	Aperture length
1 to 6	A_p	m^2 ster	47.6	52.2	17.0	Aperture
7 to 9	L_p	$\frac{\text{cm ster}}{\text{rad}}$	908	897	877	Aperture length
7 to 9	A_p	m^2 ster	18.5	20.2	6.5	Aperture

Classes	Symbol	Units	Bays 1 to 6	Bays 7 to 9	Definition
I,II & III	ξ_o	deg.	depends on mode		penetration "cut off angle"
I,II & III	ξ_g	deg.	18.1	36.2	"gap angle"
I,II & III	ξ_t	deg.	80.1	85.0	"thickness angle"
I,II & III	ξ_d	deg.	87.4	84.3	max. angle of ξ

TABLE IX. NUCLEON DECAY FRAGMENT RANGES.

Material	Fragment	Energy (MeV)	Range R_ρ (g/cm^2)	Neutrons per Unit Area Rn ($x10^{25}/cm^2$)	All Protons per Unit Area Rn ($x10^{25}/cm^2$)	Free Protons per Unit Area Rn ($x10^{25}/cm^2$)
SiO_2	$\pi^\pm$	340	168	5.07	5.07	0
SiO_2	$\mu^\pm$	369	192	5.79	5.79	0
SiO_2	$\mu^\pm$	239	116	3.50	3.50	0
SiO_2	$e^\pm$	458	59.6	1.78	1.78	0
SiO_2	$\gamma \rightarrow e^\pm$	232	45.0	1.35	1.35	0
$CH_{1.8}$	$\pi^\pm$	340	137	3.59	4.66	1.08
$CH_{1.8}$	$k^\pm$	106	12.9	.338	.438	.101
$CH_{1.8}$	$k^\pm$	100	11.8	.310	.403	.093
$CH_{1.8}$	$\mu^\pm$	369	157	4.11	5.34	1.25
$CH_{1.8}$	$\mu^\pm$	239	94.7	2.48	3.21	.74
$CH_{1.8}$	$e^\pm$	458	52.8	1.58	1.78	.20
$CH_{1.8}$	$\gamma \rightarrow e^\pm$	232	37.0	1.11	1.26	.15

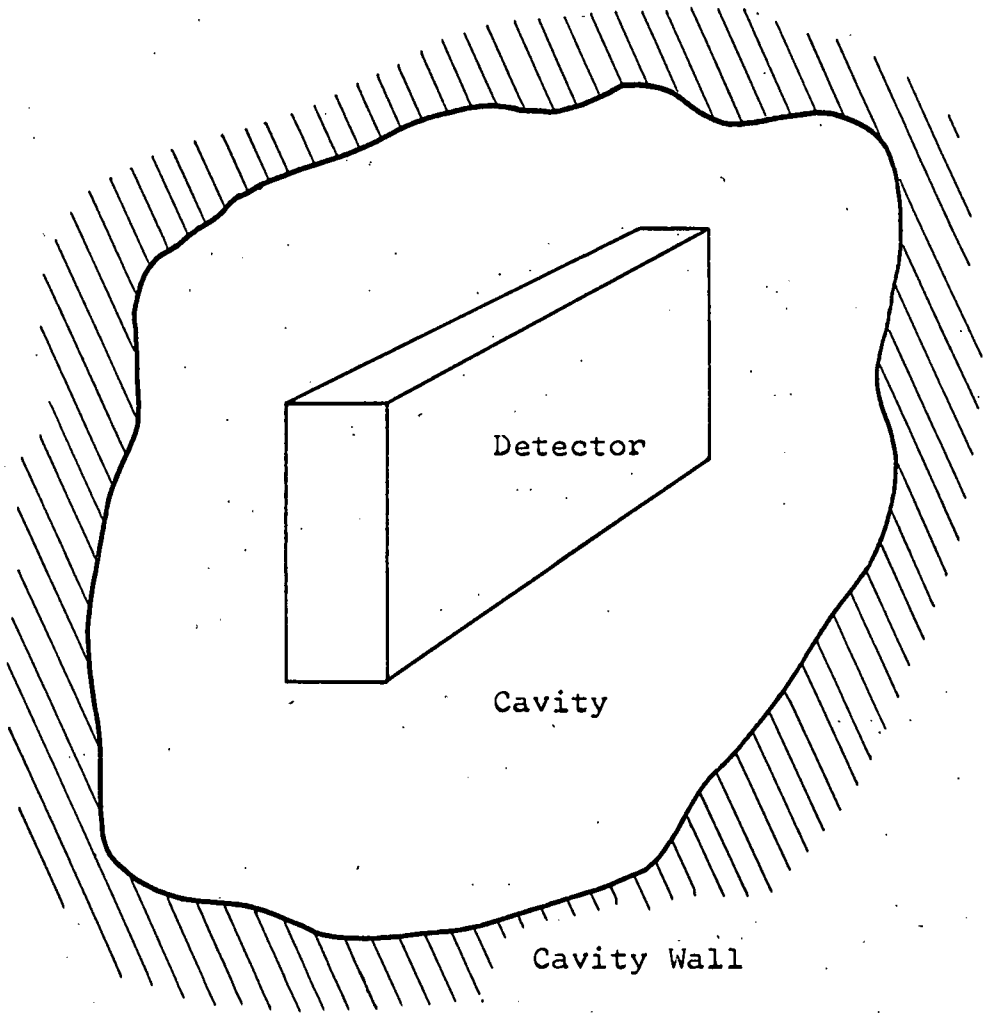

Fig. 1. Schematic Arrangement of Experiment.

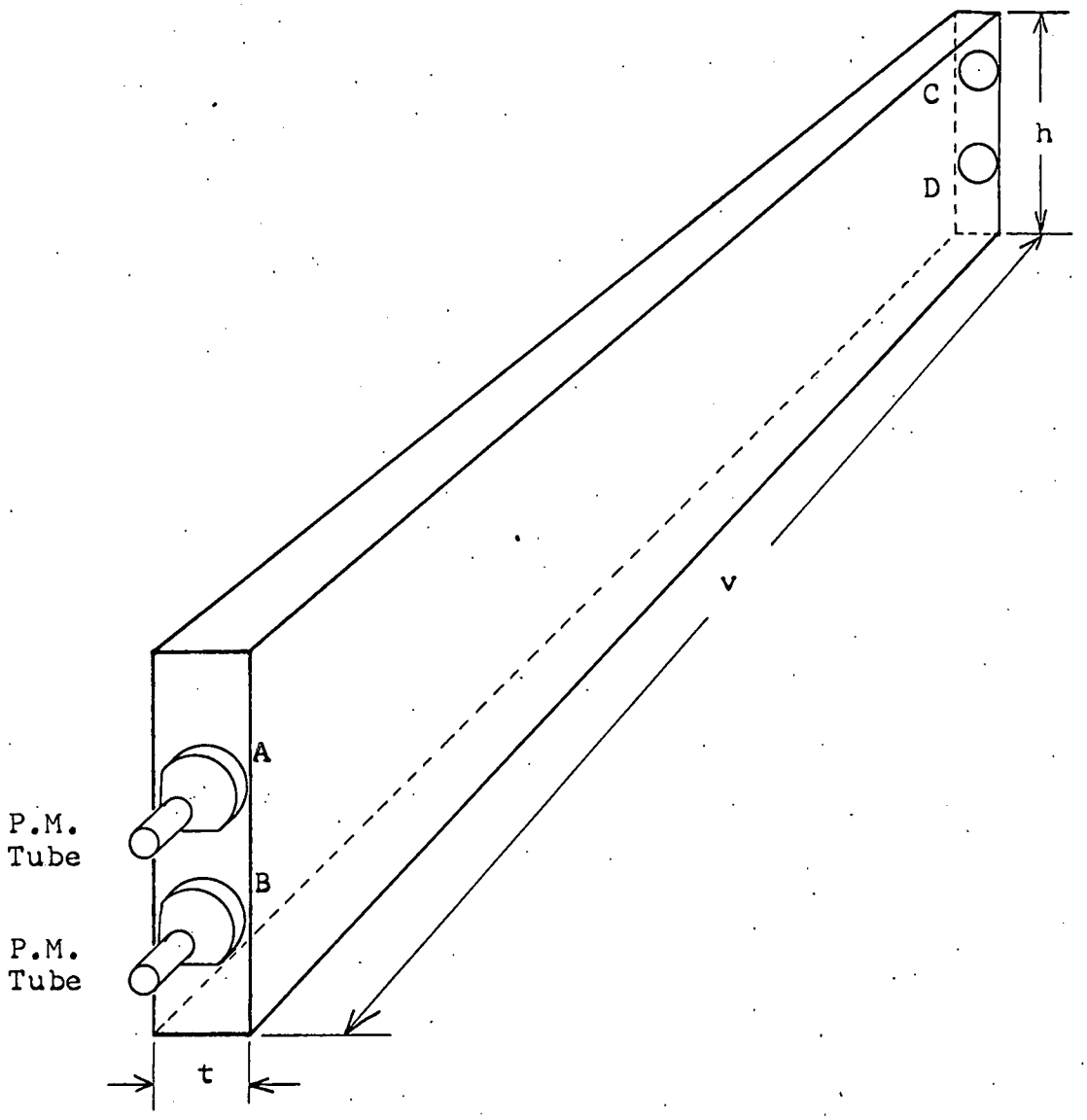

Fig. 2. Sketch of detector element.

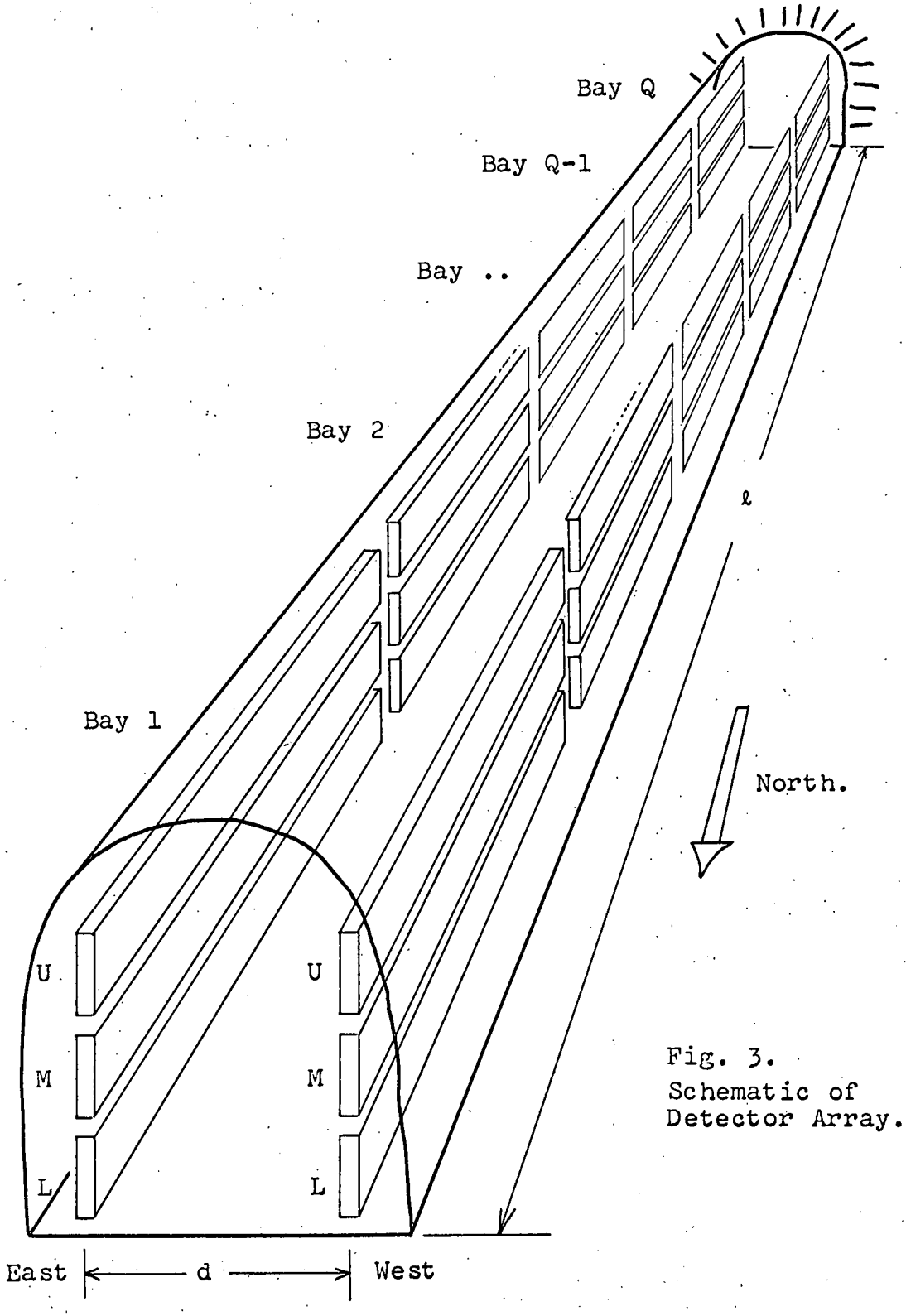

Fig. 3.
Schematic of
Detector Array.

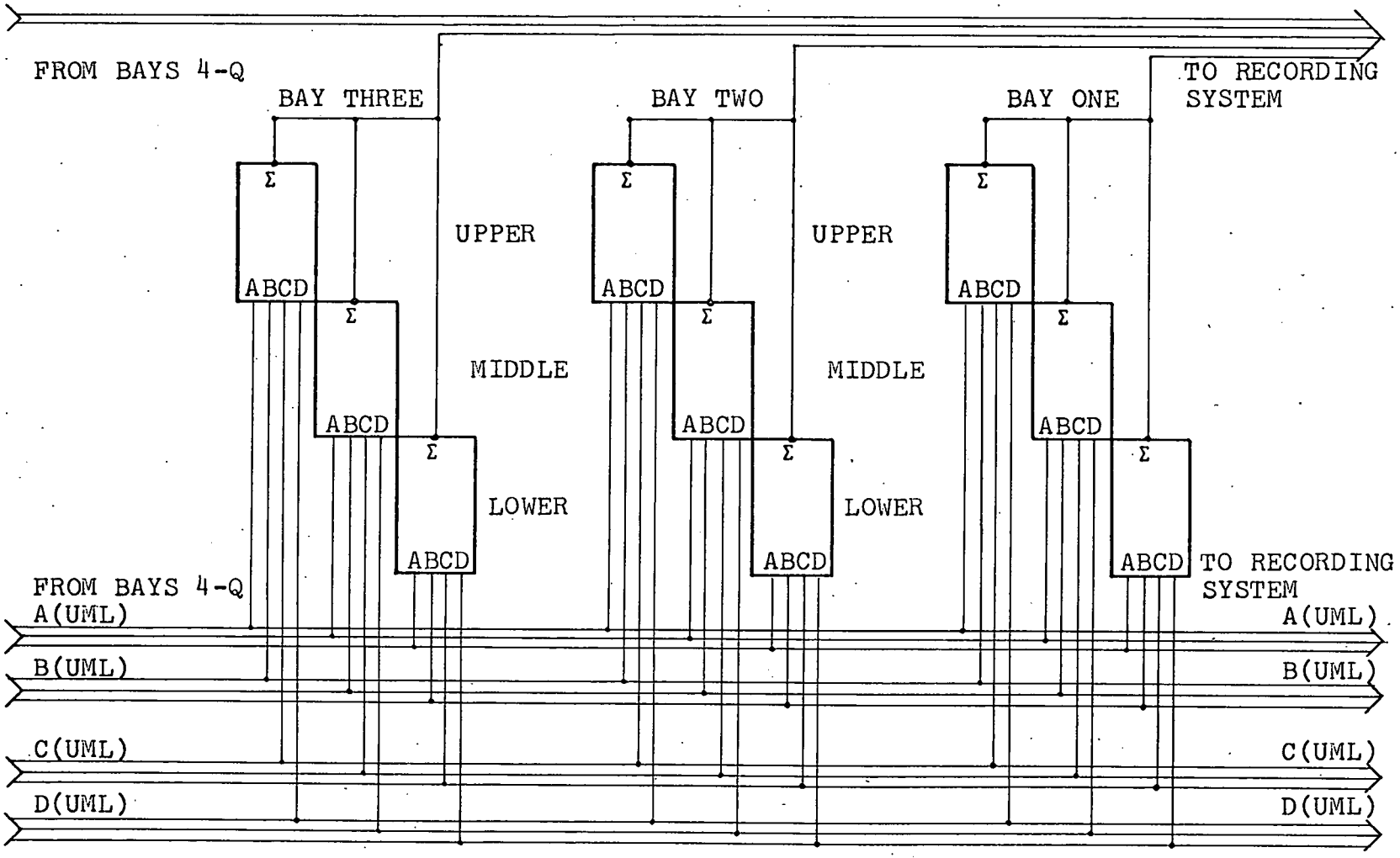

Fig. 4. Detector Electronics Schematic for one Side of Array Showing the Grouping of P.M. Signals on One Side into "Upper", "Middle", "Lower", and "Bay" Signals.

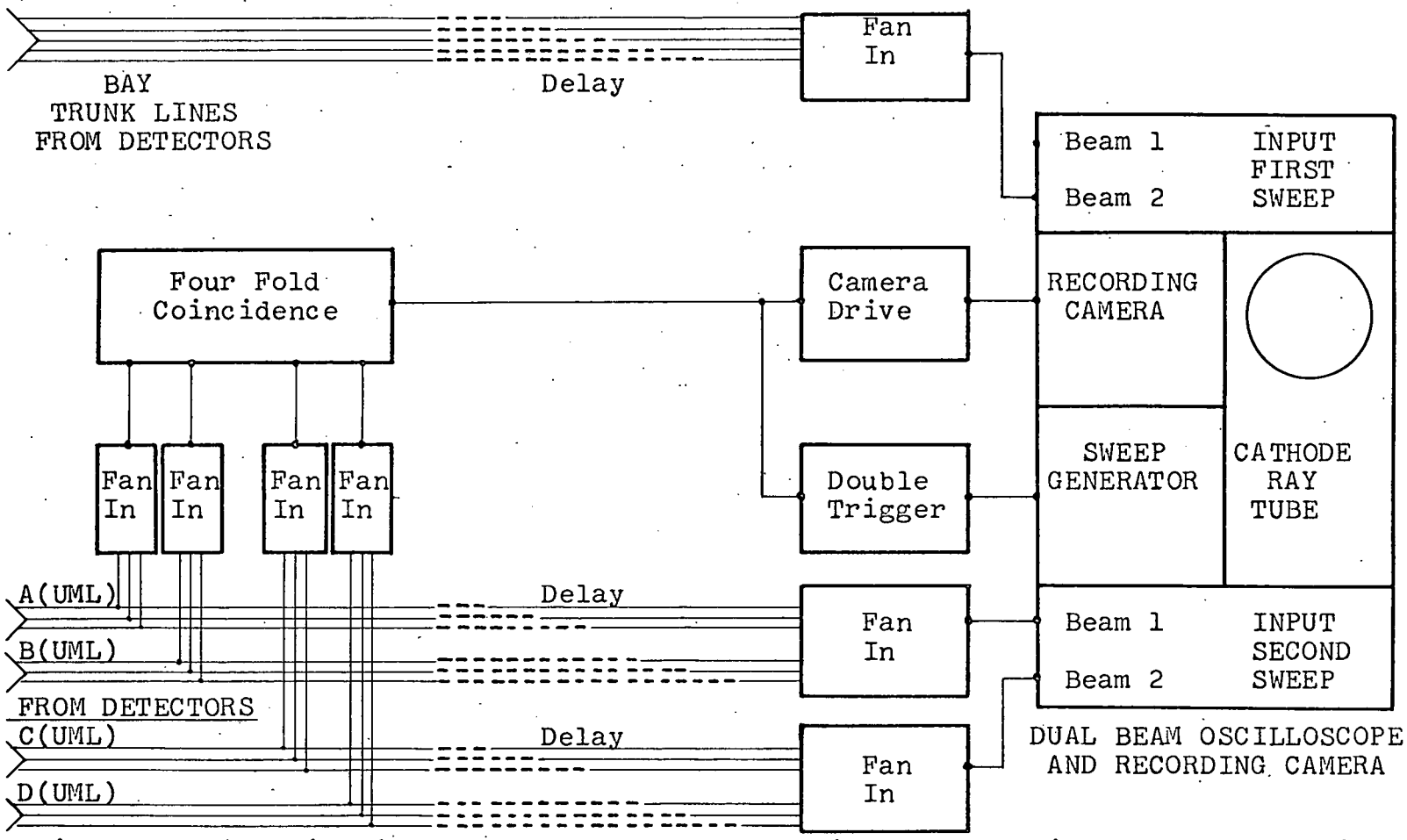

Fig. 5. Schematic Diagram of Detector Electronics For One Side of Array Showing Delay Lines, Coincidence Circuit, and Oscilloscope Recording Camera.

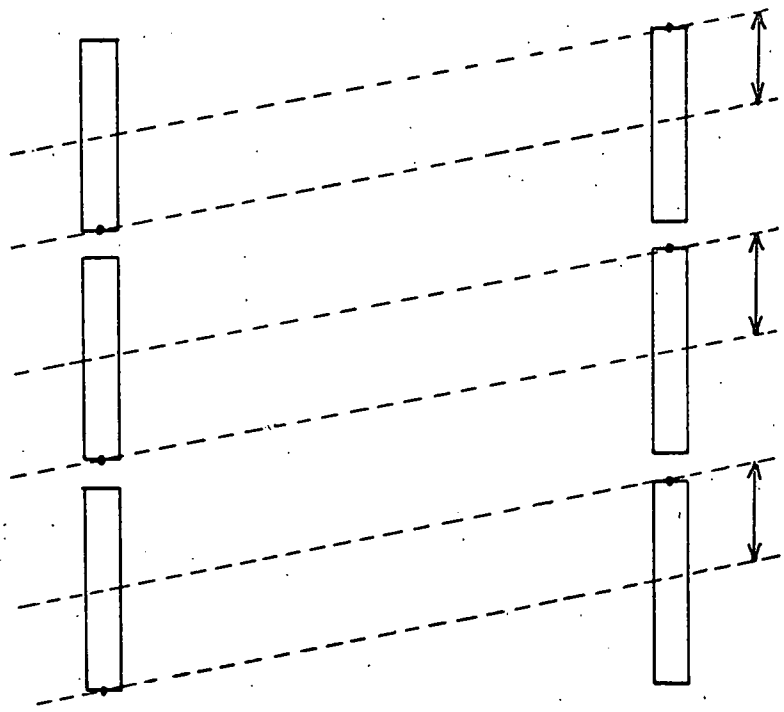

Fig. 6. Effective Height of Detectors for Class I Events (End View of Rail Elements).

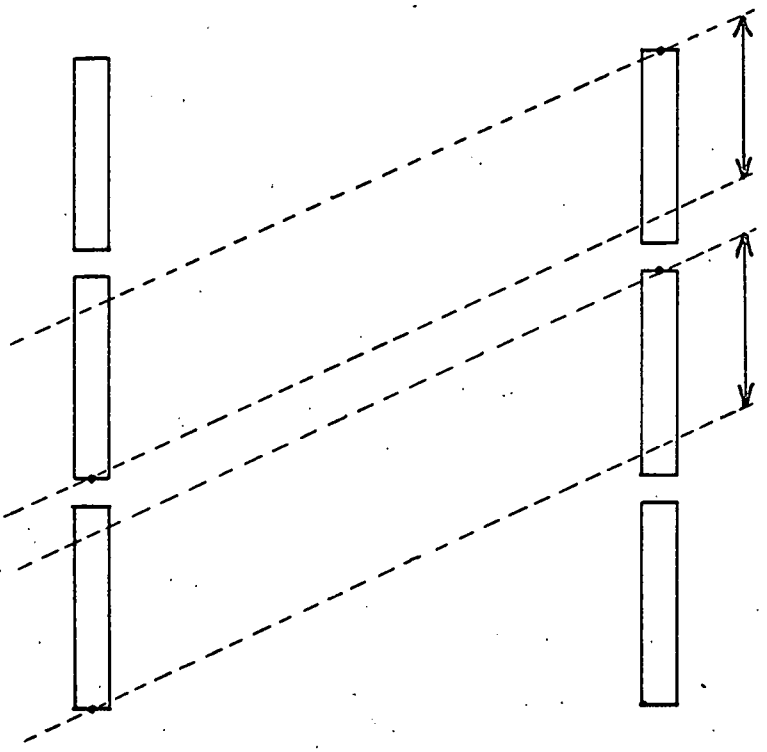

Fig. 7. Effective Height of Detectors for Class II Events (End View of Rail Elements).

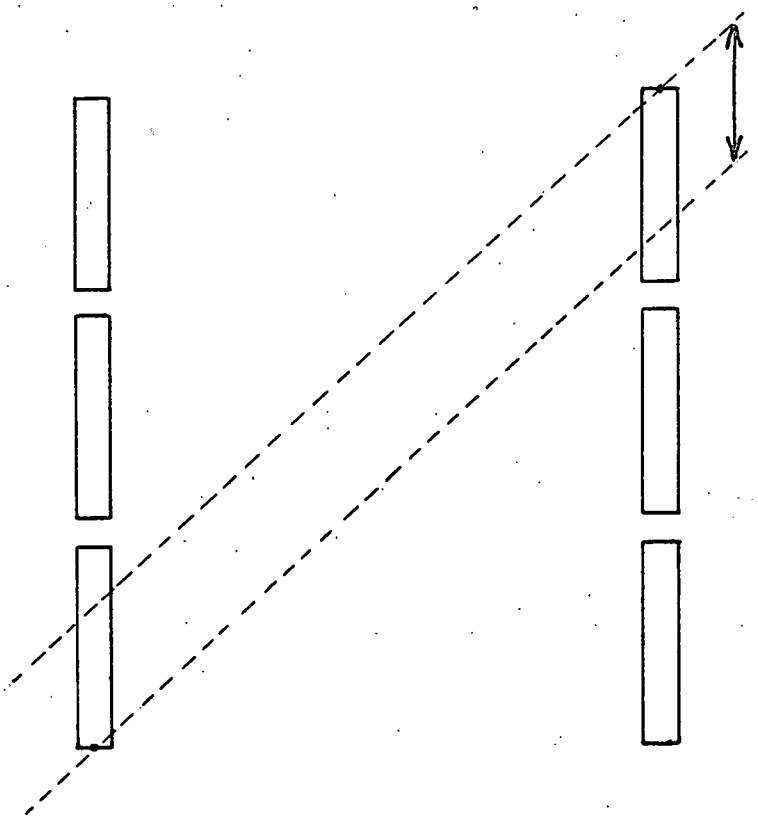

Fig. 8. Effective Height of Detectors for Class III Events (End View of Rail Elements).

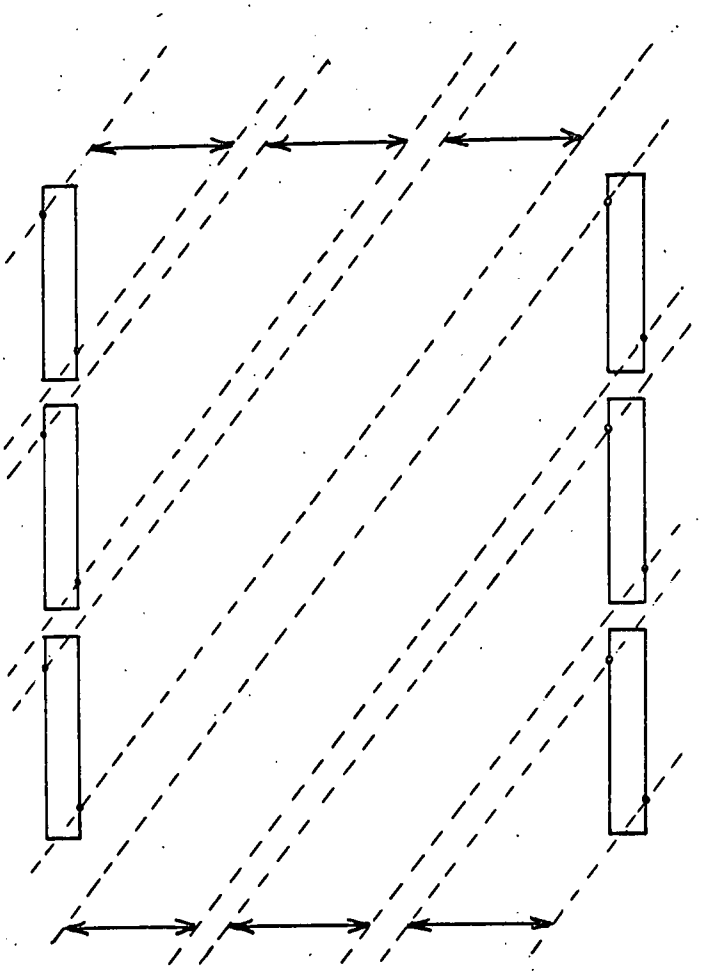

Fig. 9. Effective Width of Detectors for Class IV, Single Detector, Events (End View of Rail Elements).

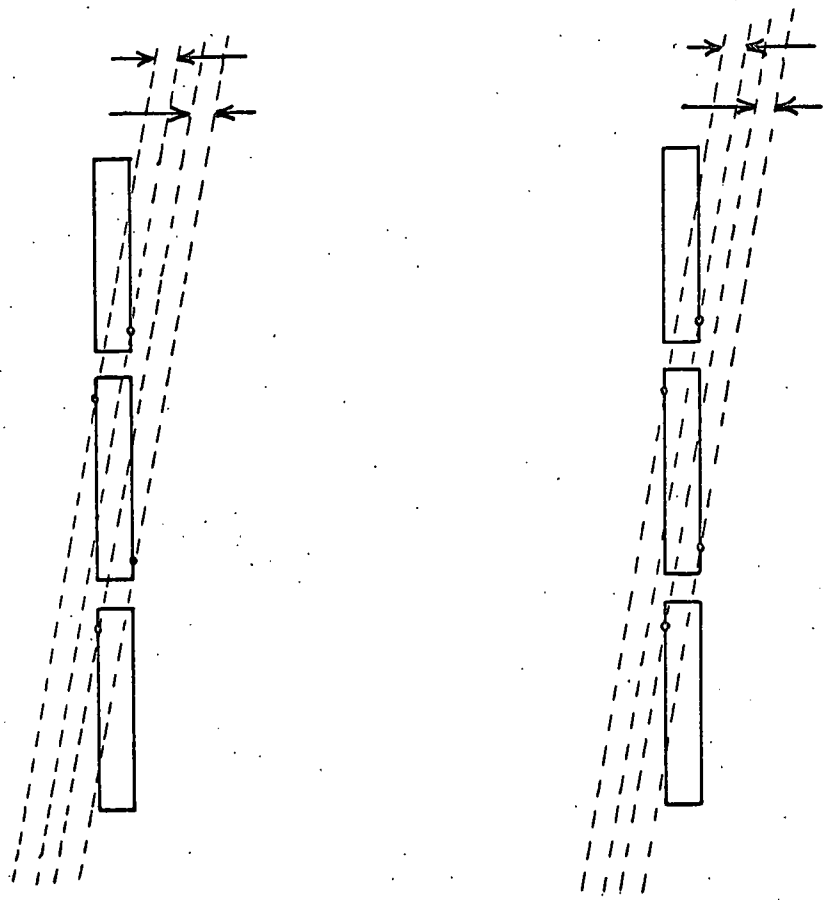

Fig. 10. Effective Width of Detectors for Class V, Double Detector, Events (End View of Rail Elements).

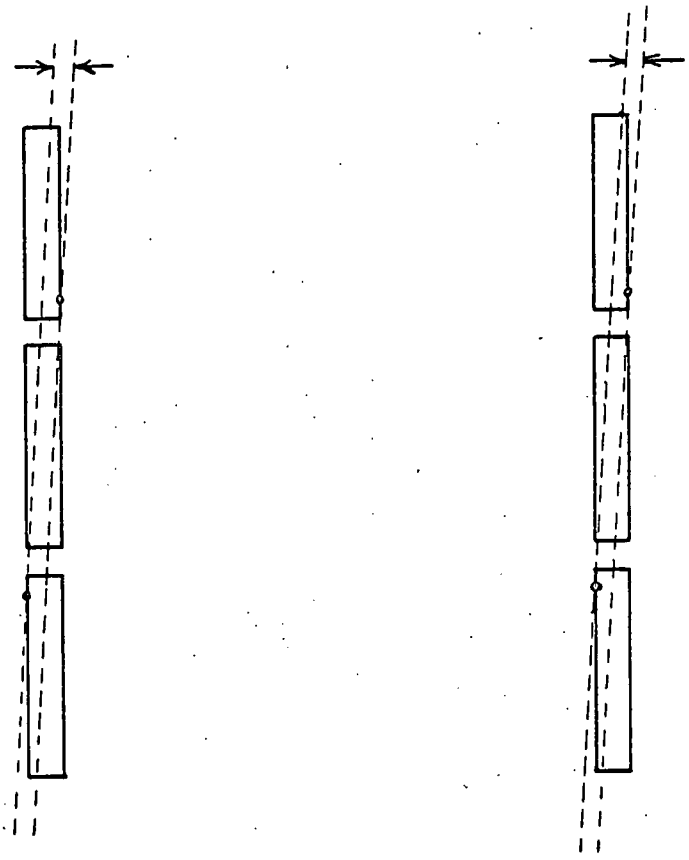

Fig. 11. Effective Width of Detectors for Class VI, Triple Detector, Events (End View of Rail Elements).

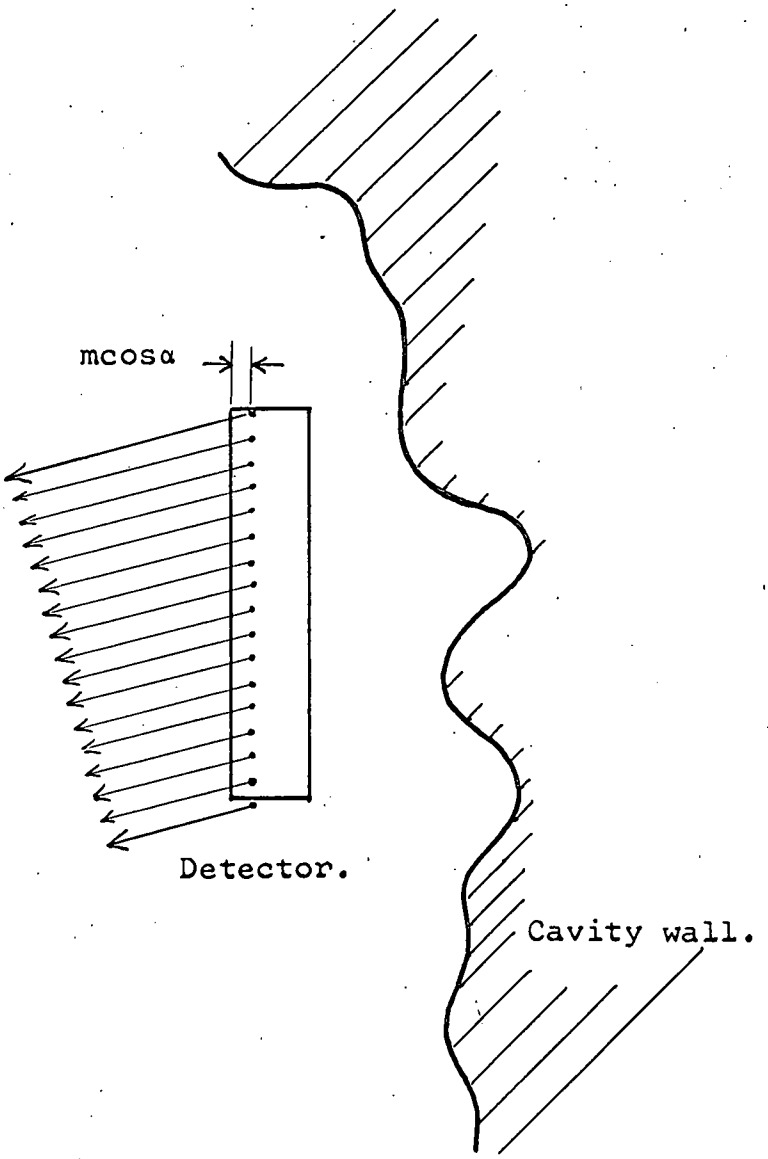

Fig. 12. Nucleon Decay Fragments at Angle (αβ) Originating Within Sensitive Region of Detector.

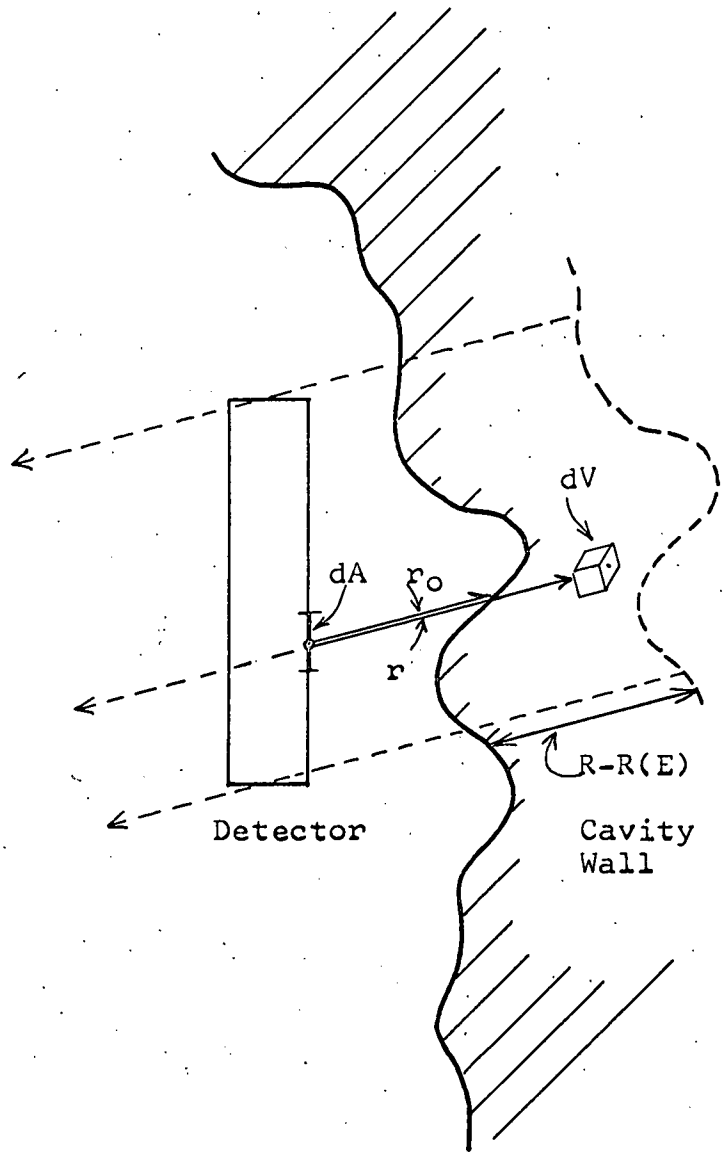

Fig. 13. Nucleon Decay Fragments At Angle ($\alpha\beta$) Originating in Volume dV and Passing Through dA.

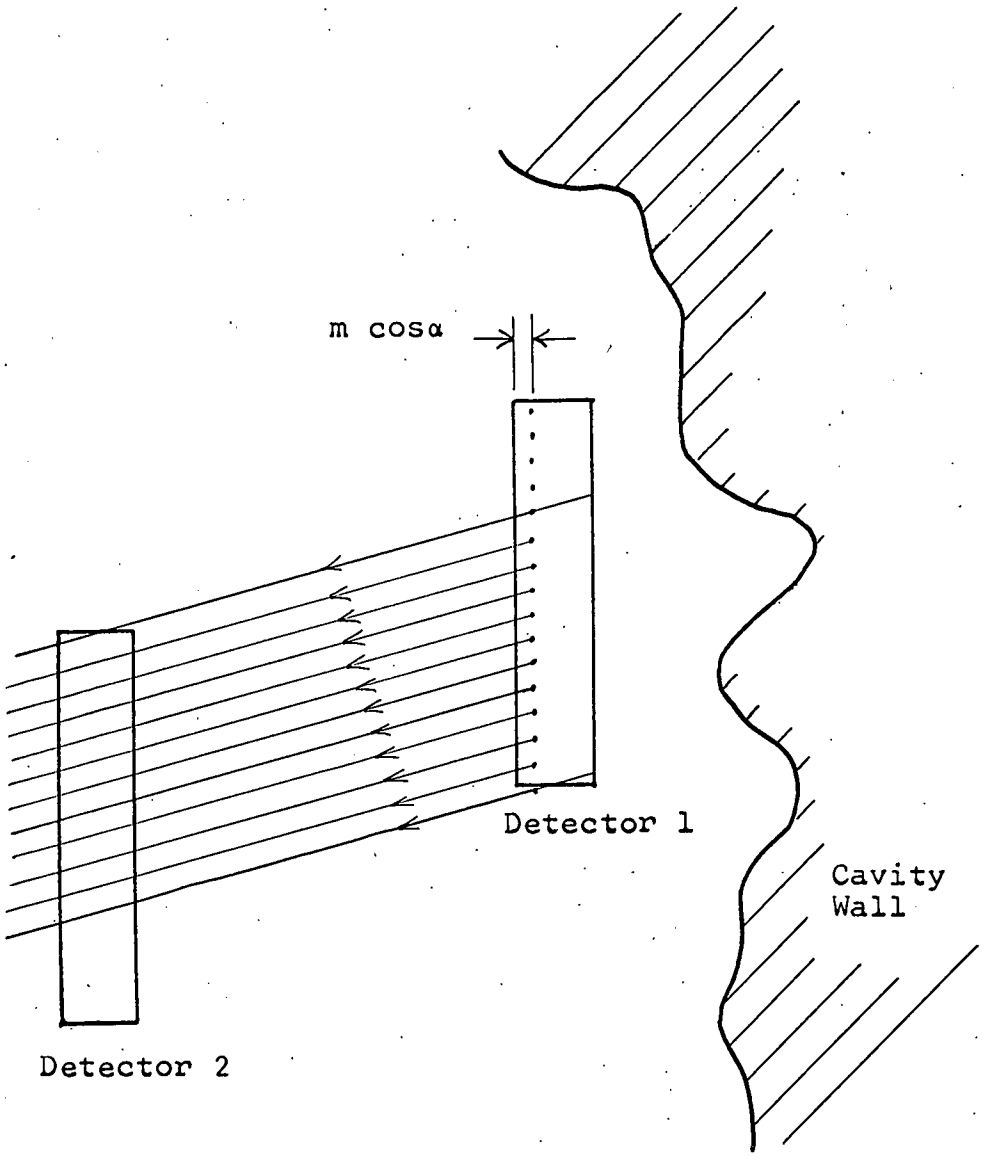

Fig. 14. Nucleon Decay Fragments at Angle ($\alpha\beta$) Originating within sensitive Region Of Detector And Passing Through Both Detectors.

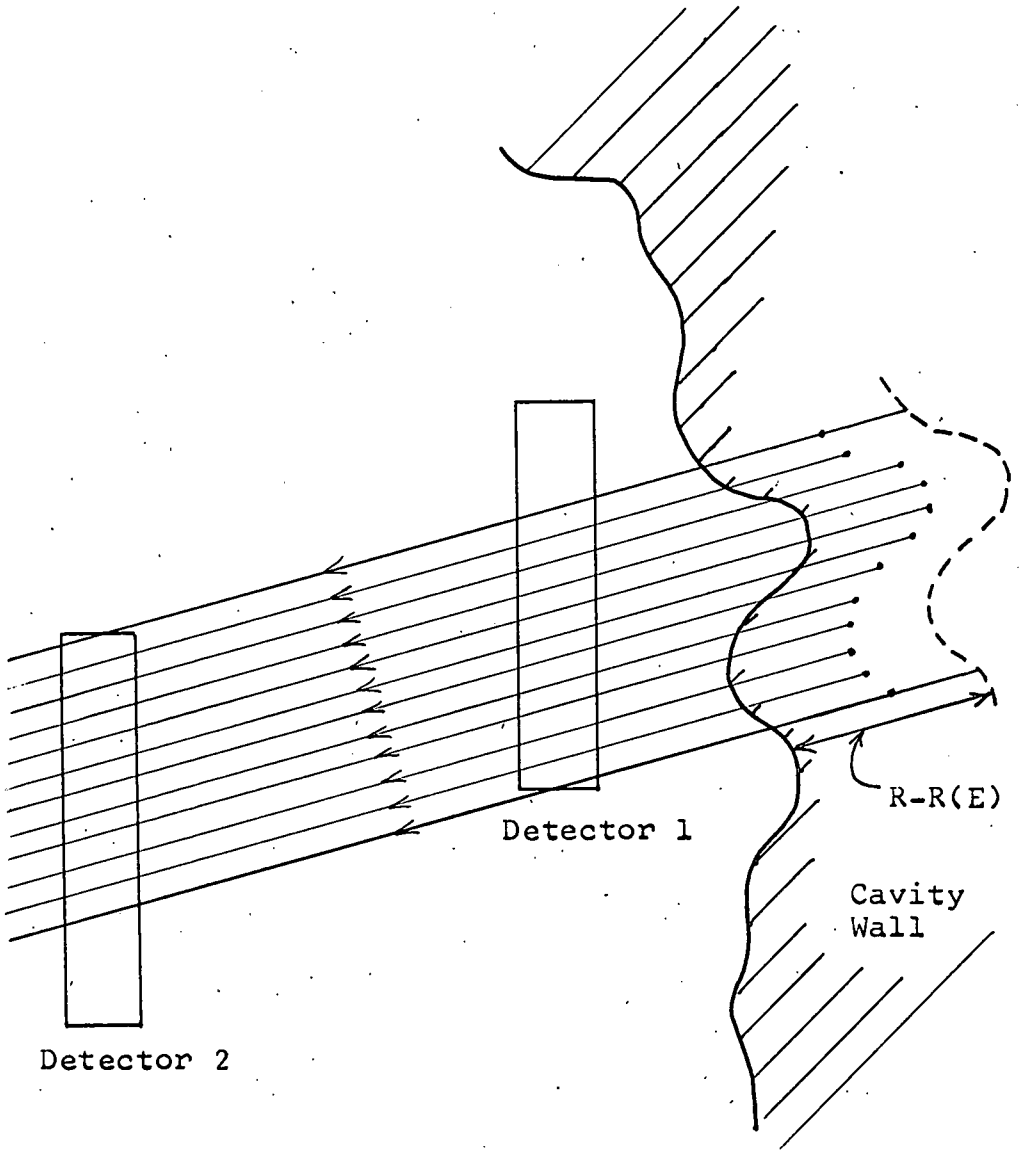

Fig. 15. Nucleon Decay Fragments at Angle ($\alpha\beta$) Originating in Wall and Passing Through Both Detectors.

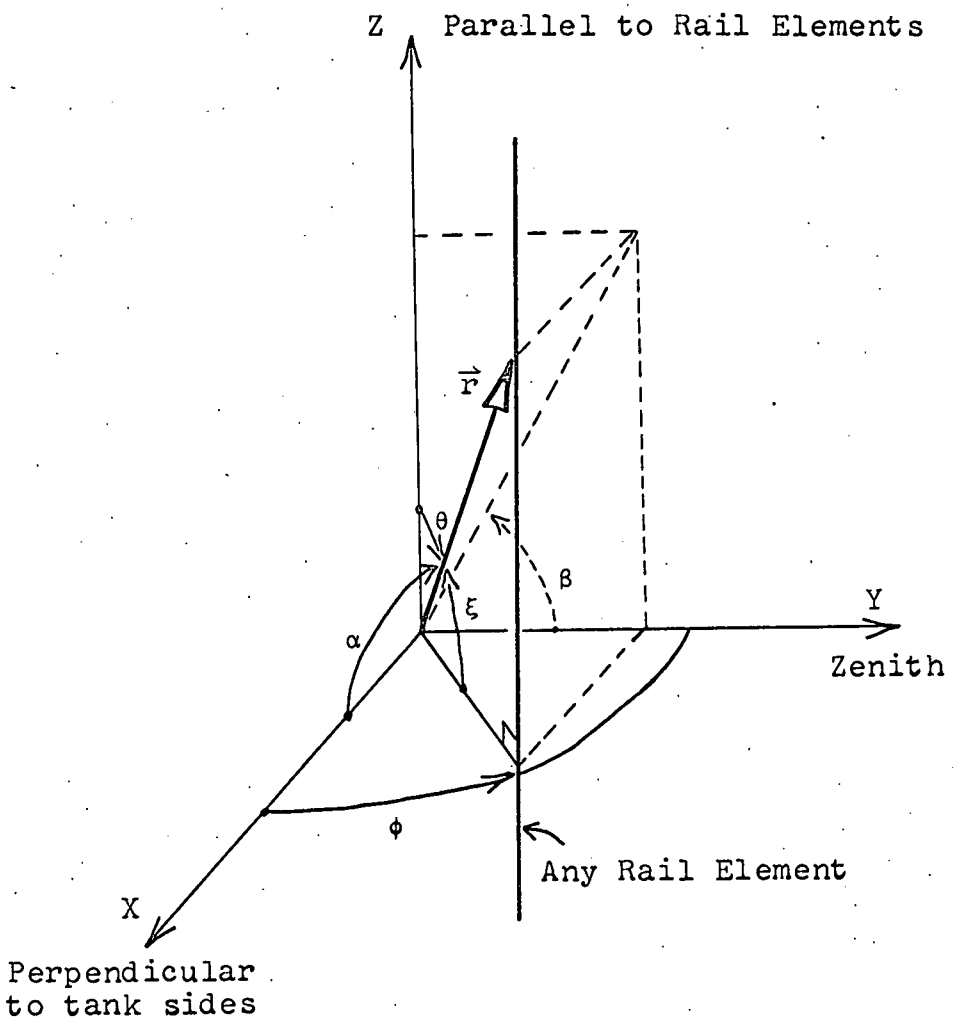

$$\xi = \pi/2 - \theta$$

$$d\Omega = \sin\theta \, d\phi \, d\theta = \cos\xi \, d\phi \, d\xi$$

$$\cos\alpha = \cos\xi \cos\phi$$

Fig. 16. Orientation Coordinate System.

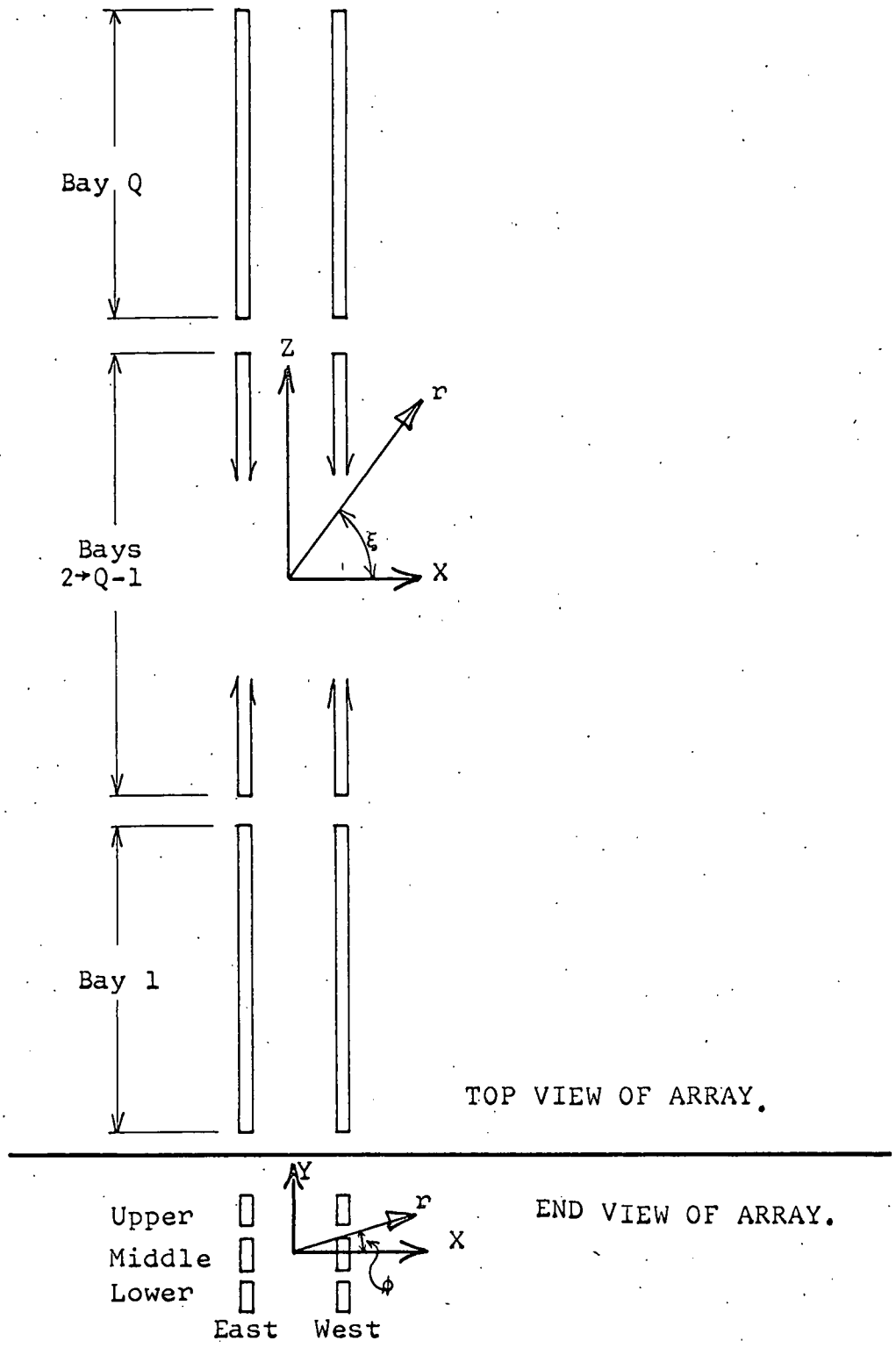

Fig. 17. Location of Origin of Coordinate System.

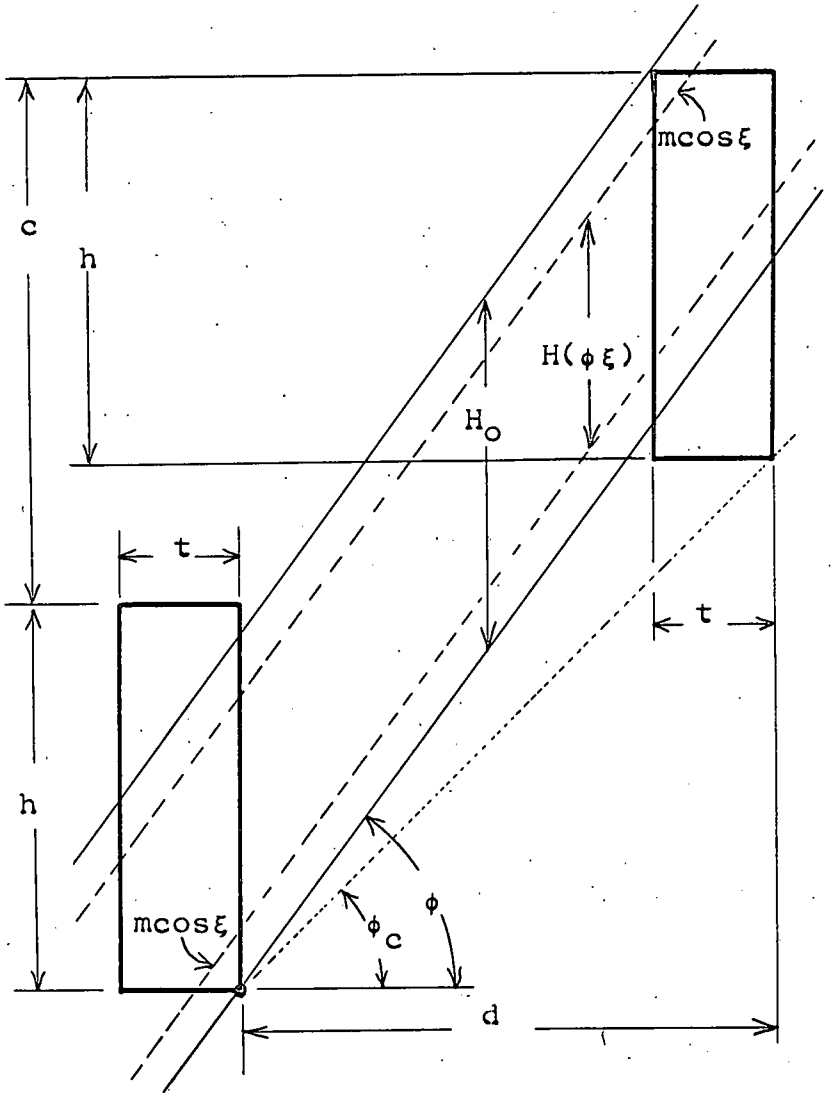

$H(\phi,\xi) = H_o - 2m\cos\xi\sin\phi$

$= \{(h+c)-(d-t)\tan\phi-2m\cos\xi\sin\phi\}$

ϕ_m = angle at which $H(\phi,\xi) = 0$. See Fig. 25.

Fig. 18. Shadow Height of Two Parallel Flat Detectors for Angles $\phi_c < \phi < \phi_m$. End View of Rail Elements.

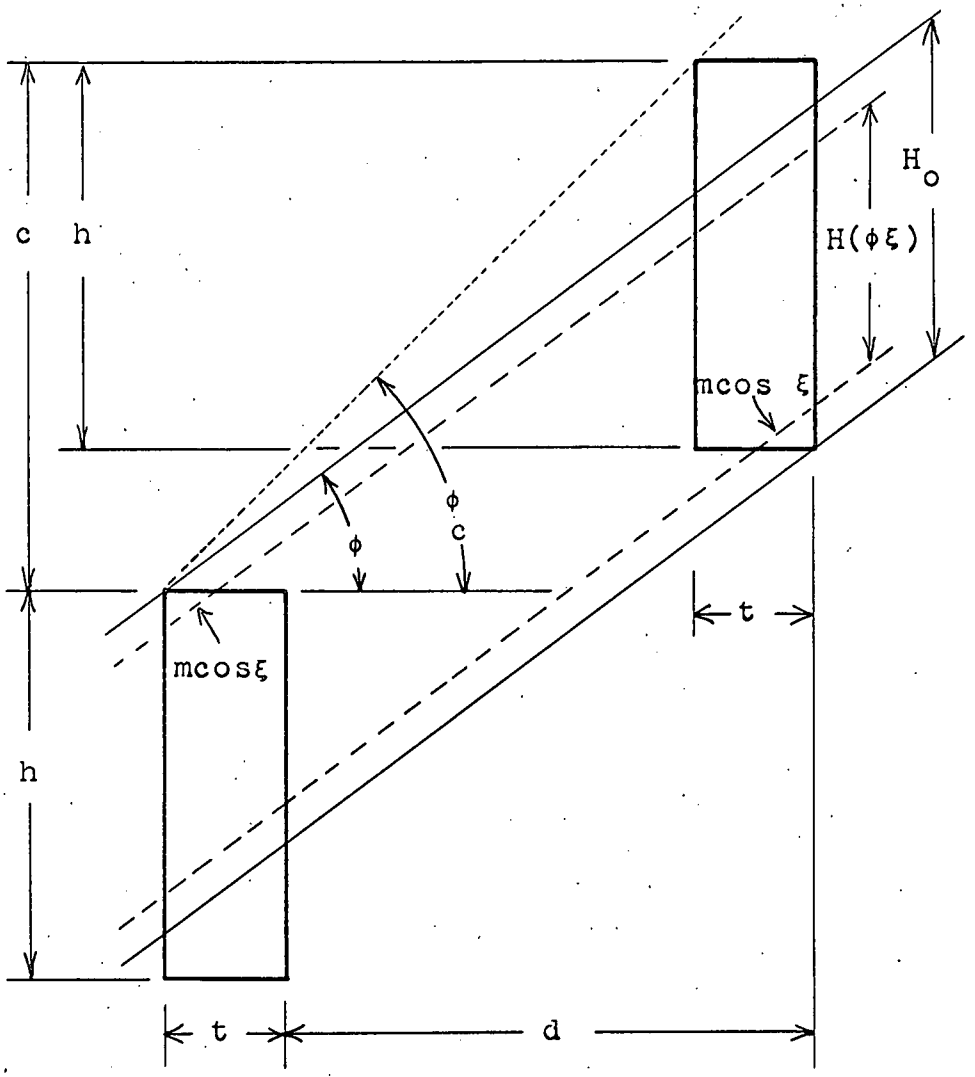

$$H(\phi\xi) = H_o - 2m\cos\xi\sin\phi =$$

$$= \left((t+d)\tan\phi-(c-h)-2m\cos\xi\sin\phi\right)$$

ϕ_n = angle at which $H(\phi,\xi) = 0$. (See Fig. 26.)

Fig. 19. Shadow Height of Two Parallel Flat Detectors for Angles $\phi_n<\phi<\phi_c$. End View of Rail Elements.

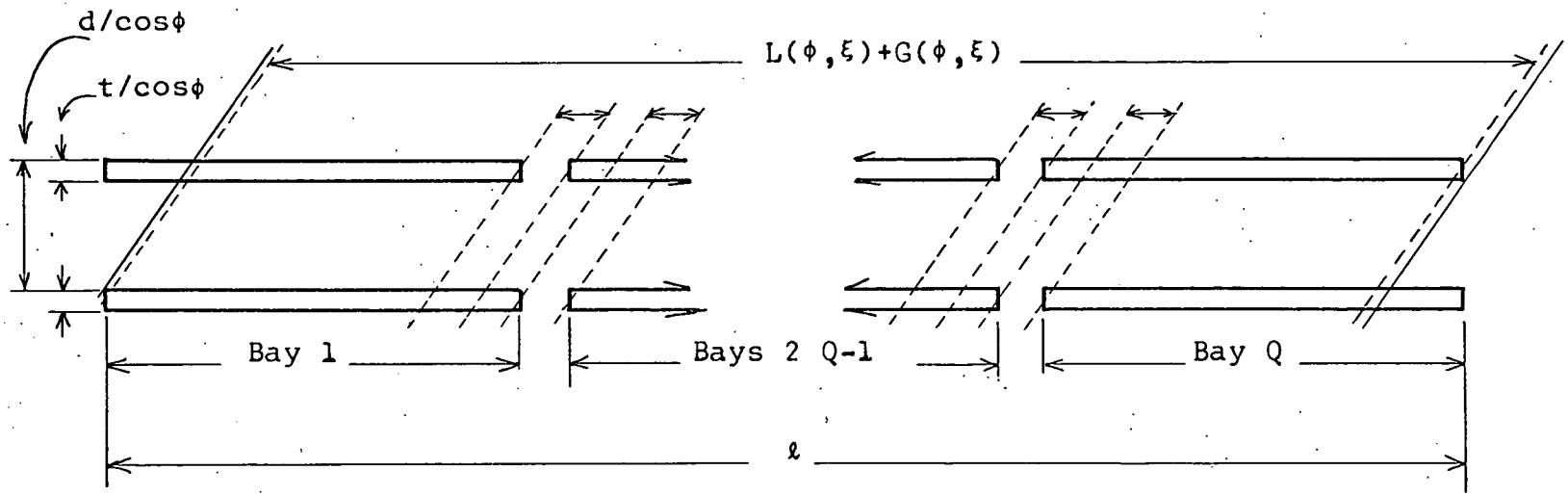

$$L(\phi,\xi) = \left(\ell - \frac{d}{\cos\phi}\tan\xi + \frac{t}{\cos\phi}\tan\xi - 2\,m\sin\xi\right) - G(\phi,\xi) \quad 0<\xi<\xi_d$$

Fig. 20. Shadow Length of Two Parallel Flat Discontinuous Rail Detectors for $0<\xi<\xi_d$. Top View of Detector Elements.

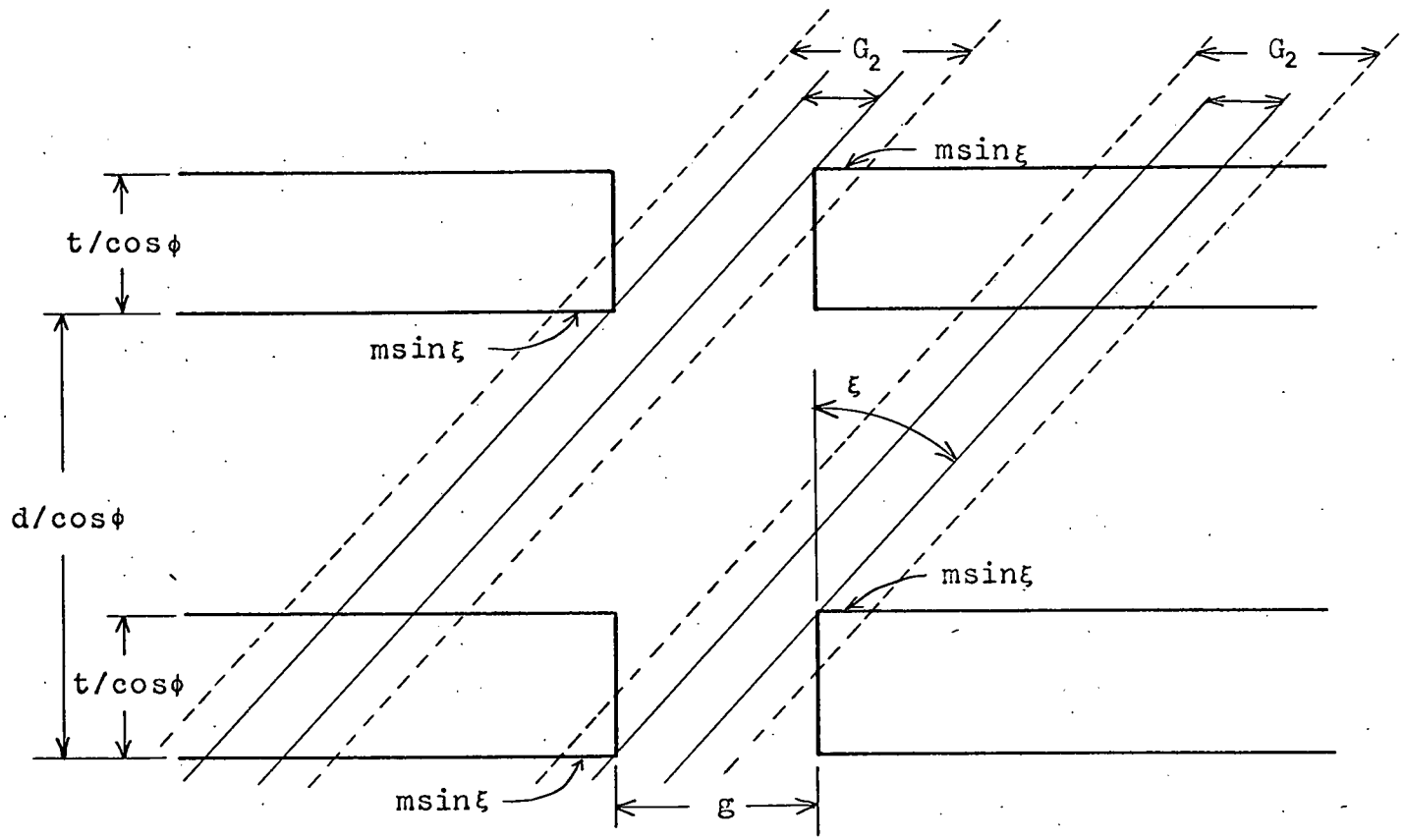

$$G(\phi,\xi) = 2(Q-1)G_2 = 2(Q-1)\left(g - t\tan\xi/\cos\phi + 2m\sin\xi\right) \quad \xi_g < \xi < \xi_t$$

$$G(\phi,\xi) = 0 \quad . \quad . \quad . \quad . \quad . \quad . \quad . \quad . \quad \xi_t < \xi < \pi/2$$

Fig. 21. Length Of Gaps For $\xi_g < \xi < \pi/2$. Top View Of Detector Elements.

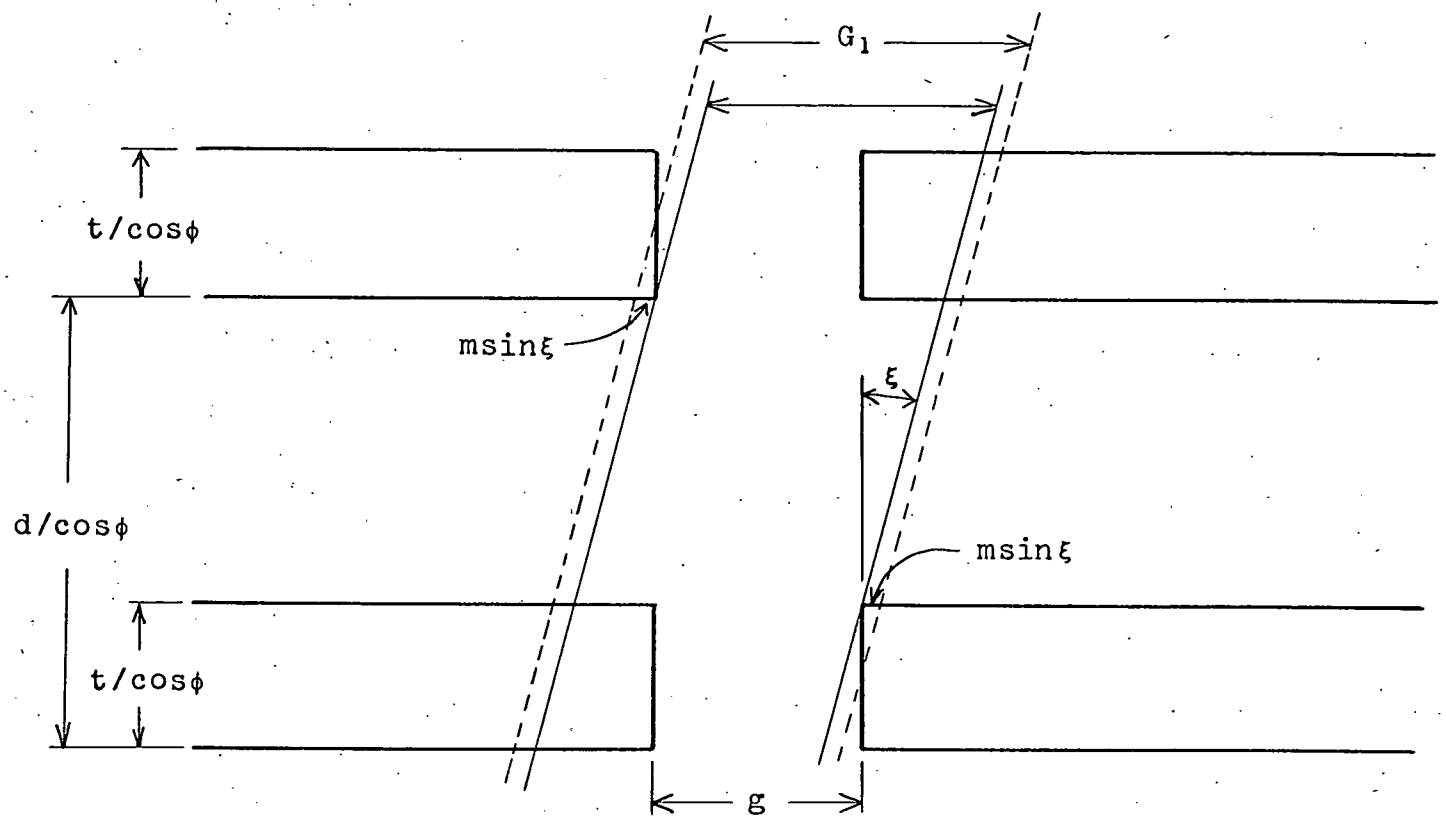

$$G(\phi,\xi) = (Q-1)G_1 = (Q-1)(g + (d-t)\tan\xi/\cos\phi + 2m\sin\xi)$$

Fig. 22. Length Of Gaps For $0<\xi<\xi_g$. Top View of Detector Elements.

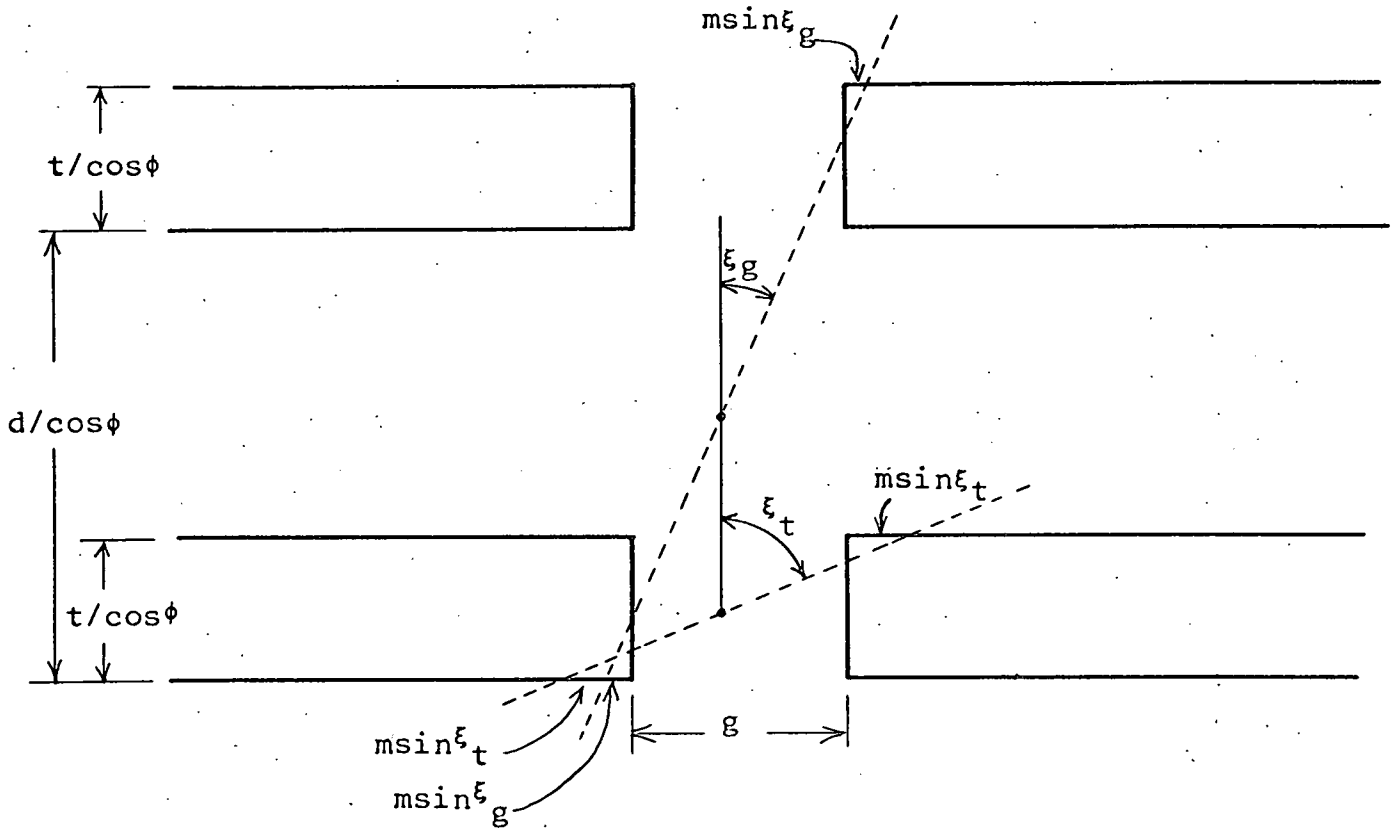

Fig. 23. Definition of ξ_g and ξ_t. Top View of Rail Elements.

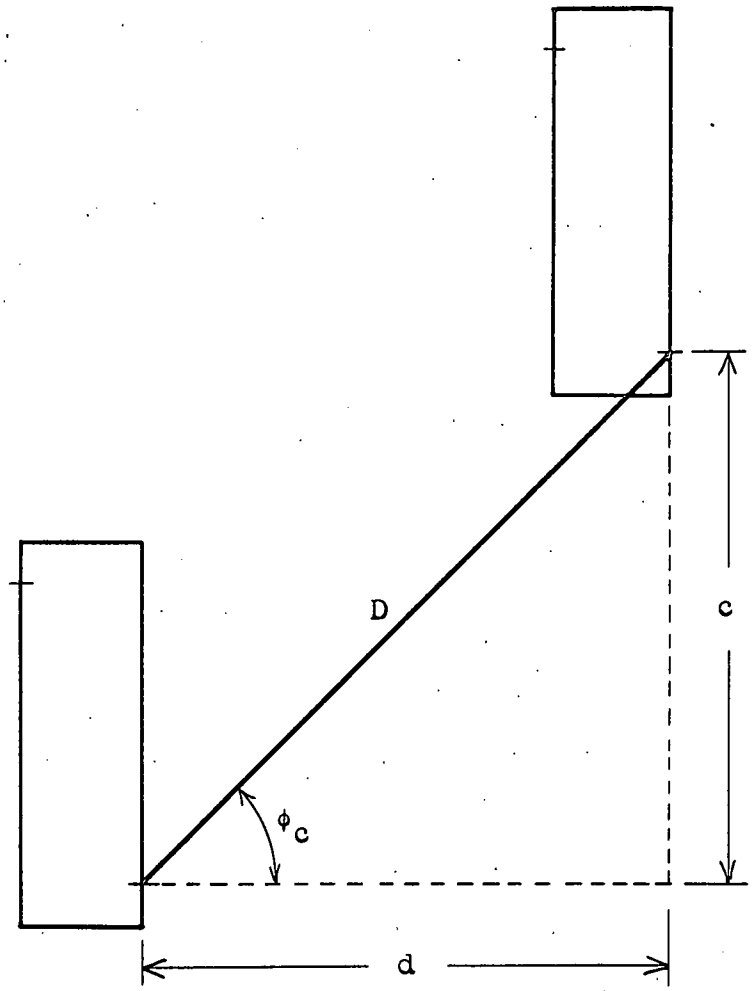

$$\tan \phi_c = \frac{c}{d}$$

$$D = d \cos\phi_c + c \sin\phi_c$$

= distance between any like points on the two detectors.

Fig. 24. Definition of ϕ_c and D (End View of Rail Elements).

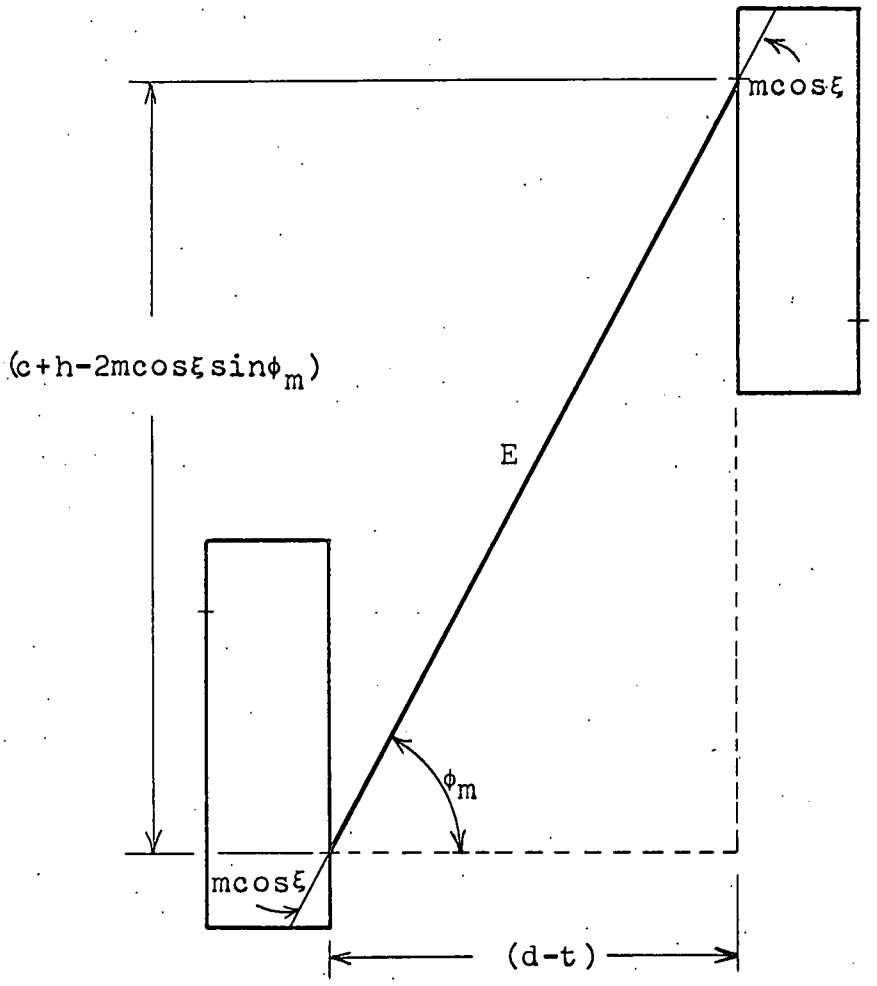

$$\tan \phi_m = \frac{(h+c-2m\cos\xi\sin\phi_m)}{d-t}$$

$$E = (d-t)\cos\phi_m + (c+h-2m\cos\xi\sin\phi_m)\sin\phi_m.$$

Fig. 25. Definition of ϕ_m and E (End View of Rail Elements).

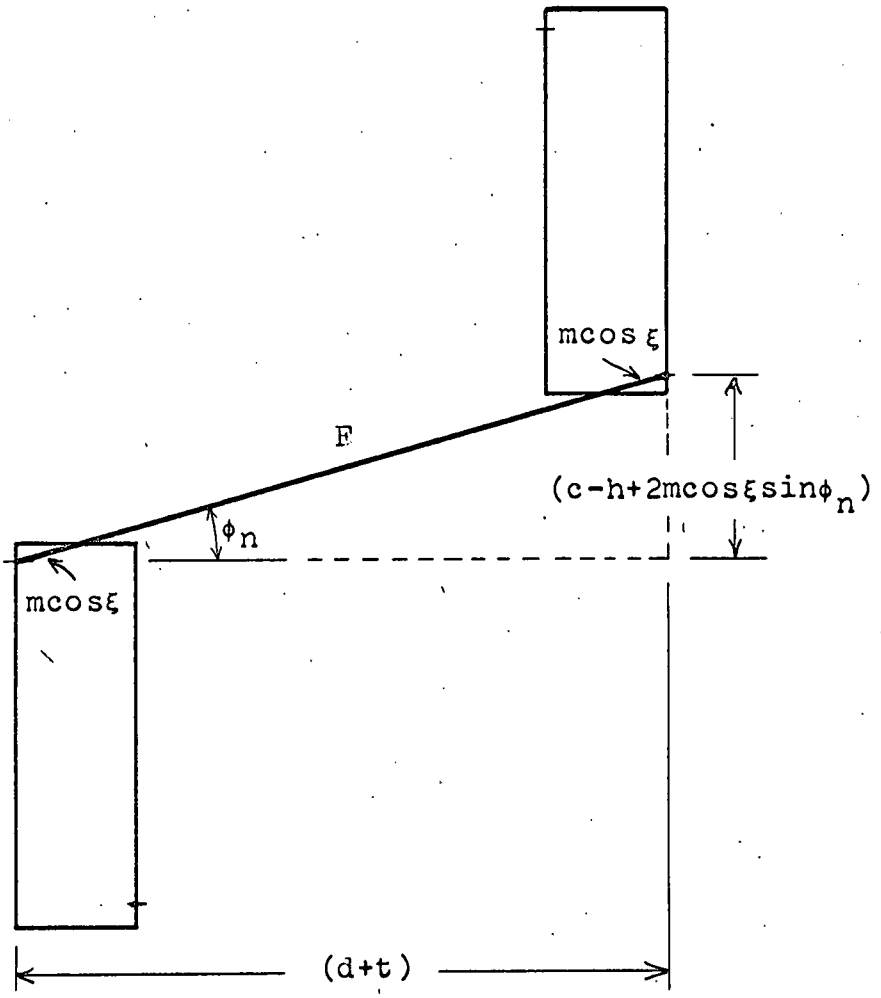

$$\tan\phi_n = \frac{(c-h+2m\cos\xi\sin\phi_n)}{d+t}$$

$$F = (d+t)\cos\phi_n + (c-h+2m\cos\xi\sin\phi_n)\sin\phi_n$$

Fig. 26. Definition of ϕ_n and F. (End View of Rail Elements).

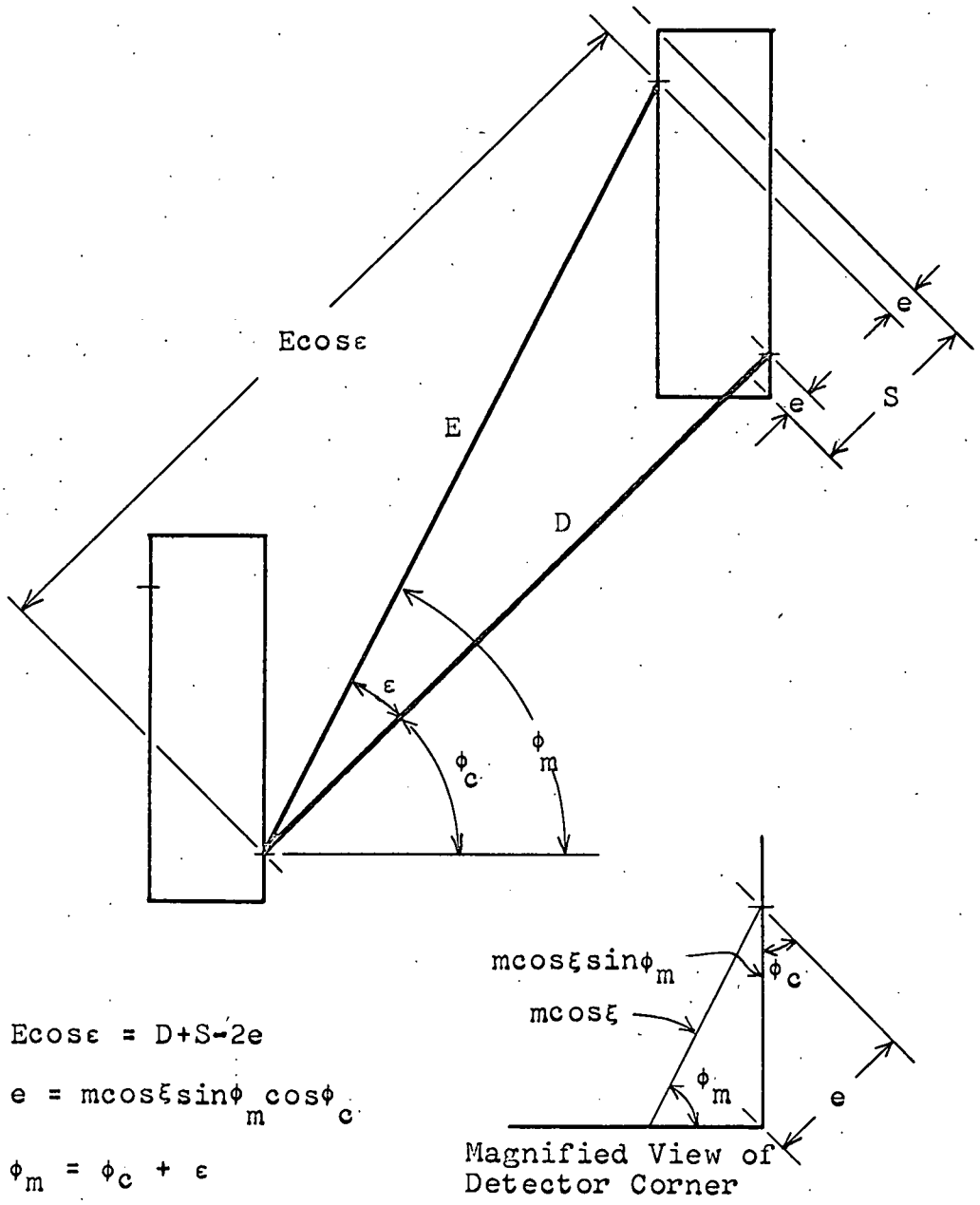

$$E\cos\varepsilon = D+S-2e$$

$$e = m\cos\xi\sin\phi_m\cos\phi_c$$

$$\phi_m = \phi_c + \varepsilon$$

Fig. 27. Definition of e, ε, and S. End View of Rail Elements. Note that E and D Intercept the Detector Elements At a Distance $m\cos\xi\sin\phi_m$ from the Top and Bottom of the Detector. See Fig. 25.

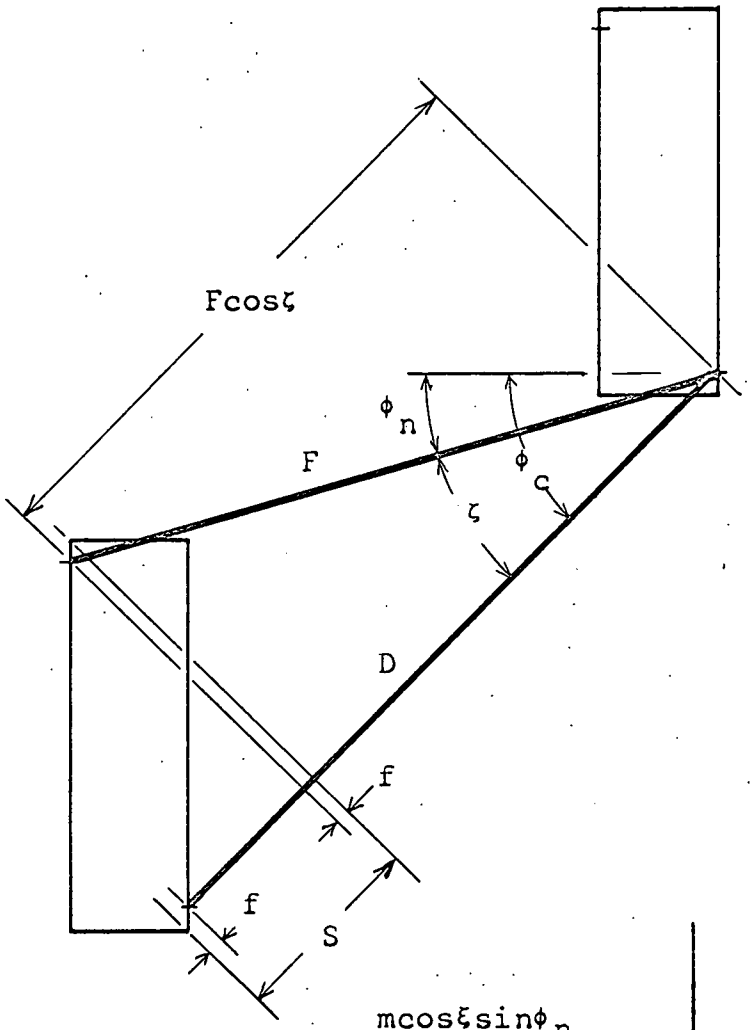

$F\cos\zeta = D-S+2f$

$f = m\cos\xi\sin\phi_n\sin\phi_c$

$\phi_n = \phi_c - \zeta$

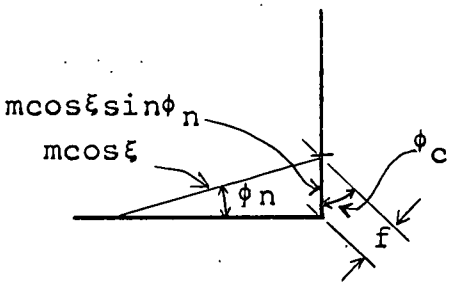

Magnified View of Detector Corner.

Fig. 28. Definition of f,ζ, and S. End View of Rail Elements. Note That E and D Interrupt the Detector Elements At a Distance $m\cos\xi\sin\phi_n$ from the Top and Bottom of the Detector, See Fig. 26.

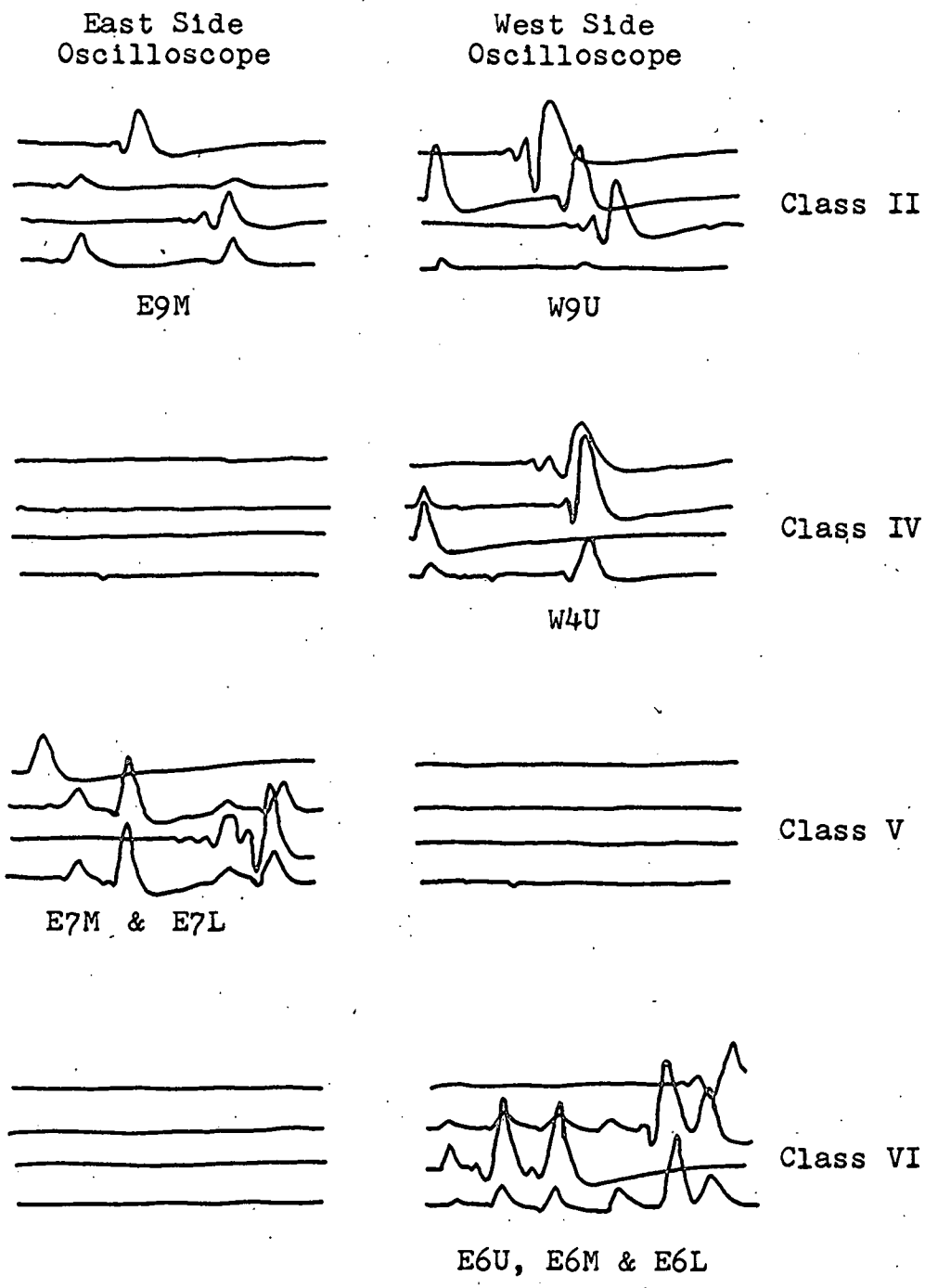

Fig. 29. Typical Oscilloscope Records of Events Involving Classes II, IV, V and VI. Detector Elements In Which More Than 10 MeV Was Deposited Are Designated By Side (East or West), Bay Number, and Position on Given Side (Upper, Middle, or Lower).